Chem Soc Rev

A Concise Guide to Sustainable PEMFCs: Recent Advances in Improving both Oxygen Reduction Catalysts and Proton Exchange Membranes

Journal:	*Chemical Society Reviews*
Manuscript ID:	CS-REV-04-2015-000302.R1
Article Type:	Review Article
Date Submitted by the Author:	03-Jun-2015
Complete List of Authors:	Scofield, Megan; Stony Brook University, Liu, Haiqing; Stony Brook University, Wong, Stanislaus

A Concise Guide to Sustainable PEMFCs: Recent Advances in Improving both Oxygen Reduction Catalysts and Proton Exchange Membranes

Megan E. Scofield[1], Haiqing Liu[1], and Stanislaus S. Wong[1,2*]

Email: stanislaus.wong@stonybrook.edu; sswong@bnl.gov

[1]Department of Chemistry, State University of New York at Stony Brook,

Stony Brook, NY 11794-3400

[2]Condensed Matter Physics and Materials Sciences Department, Building 480,

Brookhaven National Laboratory, Upton, NY 11973

*To whom correspondence should be addressed.

Abstract

With the rising interest in fuel cell vehicle (FCV) technology has emerged a growing need and realization to develop rational chemical strategies to create highly efficient, durable, and cost-effective fuel cells. Specifically, technical limitations associated with the major constituent components of the basic proton exchange membrane fuel cell (PEMFC), namely the cathode catalyst and the proton exchange membrane (PEM), have proven to be particularly demanding to overcome. Therefore, research trends within the community in recent years have focused on (i) accelerating the sluggish kinetics of the catalyst at the cathode and (ii) minimizing overall Pt content, while simultaneously (a) maximizing activity and durability as well as (b) increasing membrane proton conductivity without causing any concomitant loss in either stability or as a result of damage due to flooding. In this light, as an example, high temperature PEMFCs offer a promising avenue to improve the overall efficiency and marketability of fuel cell technology. In this Critical Review, recent advances in optimizing both cathode materials and PEMs as well as the future and peculiar challenges associated with each of these systems will be discussed.

1. Introduction to Fuel Cells and the Nature of the Problem

With recent efforts in developing alternative renewable and sustainable energy sources, there has been a rising need and interest in pursuing both basic and applied research towards building viable fuel cell (FC) configurations for a host of multi-scale platforms ranging from portable electronics, commercial and industrial buildings, residential power, to utility-scale applications. Currently, the largest practical use of fuel cells has been associated with the stationary power market. In parallel, there has been a concomitantly high level of enthusiasm for creating effective designs for commercial fuel cell vehicles (FCV). Specifically, Navigant Research, a business-consulting firm, has predicted that by the year 2017, FCV sales will surpass that of the stationary fuel cell market, with over two million FCV sales expected annually by 2030.[1]

By investing in FCVs, the objective has been to replace and provide an environmentally sustainable alternative to gasoline-powered cars, and the potential detrimental effects associated with them. Specifically, significant efforts have been expended towards devising a clean energy automotive alternative which would not require as much fossil fuel consumption, thereby mitigating for the generation of potentially harmful CO_2 emissions and greenhouse gases. However, current FCVs cost approximately $49/kW to operate as compared with the $30/kW necessary in order for this technology to be competitive with internal combustion engines.[2, 3] Therefore, using sustainable strategies, a key objective has been to create highly efficient, robust, and stable fuel cell architectures possessing an overall reduced cost, so as to promote their general competitiveness and eventual acceptance into the mass market.

A fuel cell is an electrochemical device that converts chemical energy via an oxidation process (at the anode) and a corresponding reduction (at the cathode) of a fuel into electrical energy. A variety of FCs exist, including solid oxide fuel cells (SOFC), molten carbonate fuel cells (MCFC), and proton

exchange membrane fuel cells (PEMFC), with each configuration possessing specific advantages and disadvantages.[4-6]

For example, SOFCs operate within the temperature range of 700-1000°C, which can increase the kinetics of the cell dramatically. However, due to this relatively high temperature range, a SOFC can require a longer period of time to commence and operate. Additionally, these particular FCs need to be composed of heat-resistant and durable materials. Similarly, MCFCs also operate at a relatively high temperature of between 600 and 700°C, which can also improve overall kinetics as well. However, the performance and applicability of both SOFCs and MCFCs are inhibited by limitations associated with their respective electrolytes, i.e. the use of molten carbonate salt as a liquid electrolyte in MCFCs and ceramic compounds as a solid electrolyte in SOFCs, the need for CO_2 to be injected into the cathode, and issues associated with heat corrosion. As a result, both FC types are more suitable for stationary as opposed to mobile applications. In terms of overall "typical" capital (i.e. equipment and installation) costs for interconnected grid applications, activation and proper functioning of a MCFC necessitated $4,600/kW in 2014, accounting for complete installation, equipment, and labor charges. For PEMFCs and SOFCs, the corresponding costs were ~$22,000/kW and $23,000/kW , respectively, according to ICF International, a relevant consulting firm.[5] The high expenses associated with the proper operation of both PEMFCs and SOFCs strongly suggest that significant work and effort need to be expended to render these FCs as commercially viable platforms.

Typically, FCVs employ a fuel cell configuration, known as a proton exchange membrane fuel cell. A representative, conventional PEMFC membrane electrode assembly (MEA) is shown in Figure 1. Typically, in this example, hydrogen gas is supplied to the anode, where protons are generated that subsequently migrate to the cathode through the mediation of the proton exchange membrane (PEM). Electrons are also produced, that travel by means of the external load to the cathode. Subsequently, the protons combine with incoming O_2 molecules to produce H_2O, electrical energy, and heat.

FCVs utilize a PEMFC as a foundational technology due to its rapid 'start up' capabilities, 'low temperature' operation, reasonable durability, low 'weight-to-power production' ratio, and efficient responsiveness to changes in demands for power, all of which are highly advantageous attributes for both transportation and portable applications.[5] Nonetheless, this type of fuel cell configuration still requires an immense amount of research work and effort in order to reduce the cost necessary to render it commercially competitive with internal combustion engines (ICE). Therefore, this Critical Review will specifically focus on a complementary and interesting suite of efforts to chemically optimize and improve upon the two most costly and problematic components within the PEMFC, namely (a) the cathode catalyst and (b) the proton exchange membrane (PEM) itself.

In PEMFCs, the oxygen reduction reaction (ORR), localized at the cathode, requires higher overpotentials in order to initiate the reaction as compared with the hydrogen oxidation reaction (HOR) occurring at the anode, and therefore denotes the limiting 'step', as it were, in PEMFCs.[7] In other words, the process required to initiate the oxygen reduction reaction is very energy intensive. As a result, the development of new and more effective electrocatalysts at the cathode has received comparatively greater research and developmental attention as compared with analogous anode electrocatalysts.[8-10] Typically, commercial cathode catalysts are Pt-based, since elemental Pt exhibits the best activities as compared with any other metal tested. However, although these Pt catalysts can achieve high ORR activities, they suffer from serious deficiencies. Some of these shortfalls involve possible reduction, poisoning of the active site by CO due to methanol crossover, as well as catalyst ripening and dissolution, all of which practically contribute to the effective inhibition of catalytic activity. Furthermore, Pt is expensive (> $1000 per ounce) and scarce, resulting in legitimate concern for its broad applicability and commercialization on a mass scale. In particular, current FCVs, employing a PEMFC, require ~30 grams of Pt,[11] which can potentially equate to thousands of dollars of cost and contributes to a significant amount of the full cost of the PEMFC itself. Nevertheless,

progress has been made in minimizing precious metal catalyst use and incorporation. For instance, since 2007, General Motors has been able to reduce the content of Pt within their catalysts from 80 grams to less than 10 grams. Additionally, since 2008, the cost of manufacturing PEMFCs, according to Toyota, has dropped by nearly 95%, thereby indicating a significant leap forward towards practical commercialization.[12]

The commercial PEM most often employed, on the other hand, is Nafion, which is a perfluorosulfonic acid (PFSA) ionomer. This PFSA membrane is composed of a hydrophobic poly(tetra-fluoroethylene) (PTFE) backbone, which can promote reasonable mechanical stability, coupled with hydrophilic sulfonic acid side chains, thereby enhancing proton conductivity under full hydration conditions. Overall, this membrane has been employed as the commercial standard, due to its high chemical and electrochemical stabilities as well as its exceptional proton conductivity.

However, despite the research performed over the years towards improving proton conductivity, reducing material costs by producing thinner membranes, and improving membrane robustness by incorporating additives,[12] major drawbacks of PEMs still exist, especially in the context of their instability and decreased proton conductivity at high temperatures and relatively low humidities (RH). Specifically, outside the temperature range of 0 to 100°C, the proton conductivity decreases, because of the respective freezing and boiling of water. As a result, PFSA membranes necessitate a costly humidification system in order to function under optimal conditions. However, with the water provided by the humidification system, coupled with the additional water generated as a byproduct of intrinsic fuel cell chemical reactions, cathode flooding can potentially occur during normal operations, thereby causing further FC degradation.[13, 14] Therefore, by finding rational routes for chemically creating membrane materials capable of operating not only under high temperatures but also at low RH conditions to replace conventional materials and thereby completely obviate the need for a

humidification system, such synthetic advances will render FCs more commercially attractive not only for mobile FCVs but also for stationary applications.

The primary approach taken thus far to alleviate both of these significant problems has been to raise the operating temperature of the PEMFC above 80°C to a range of 120-150°C. Raising the temperature can accelerate the sluggish kinetics at the cathode, improve the CO tolerance of the electrodes, and potentially promote better 'water management' by the membrane by removing the need for a humidification system and its concomitant flooding issues. However, this strategy raises additional obstacles that need to be addressed. For instance, these conditions can significantly reduce catalyst stability and increase catalyst aggregation. Additionally, the proton conductivity of the PFSA membrane can drop dramatically along with its water retention capacity, due to the decreased amount of water molecules which would be present and responsible for the creation of interconnected pathways for proton transport.

Therefore, the purpose of each subsection as well as the entirety of this Review, which is meant to be an illustrative and thoughtful survey of existing and future directions, will be to probe salient examples and to provide for conceptual 'highlights', denoting the current 'state-of-the-art' thinking and strategies in the field. In so doing, our objective will be to explain and analyze the various chemical advances and directions aimed at the rational design and targeted performance improvement for both cathode catalysts and PEMs, respectively.

2. Advances in Catalyst Design

2.1. Oxygen Reduction Reaction (ORR) and ORR catalysts

In a fuel cell, oxygen (O_2) is electrochemically reduced at the cathode through the mediation of the oxygen reduction reaction (ORR). Fundamentally, the mechanism of oxygen reduction reaction in

acidic media involves either the direct 4-electron reduction pathway from O_2 to produce H_2O or the 2-electron reduction pathway from O_2 to form hydrogen peroxide (H_2O_2) in one of the steps:

$$O_2 + 4\ H^+ + 4\ e^- \rightarrow 2\ H_2O \text{ (four-electron pathway)}$$

$$O_2 + 4\ H^+ + 4\ e^- \rightarrow H_2O_2 + 2\ H^+ + 2\ e^- \rightarrow 2\ H_2O \text{ (two-electron pathway)}$$

Water is directly produced when oxygen is reduced through the four-electron reduction mechanism. On the other hand, the two-electron reduction occurs at low potentials and produces hydrogen peroxide as an intermediate byproduct. As previously alluded to, the most commonly employed metal in catalysts for ORR in acidic media is Pt, due to its ability to reduce oxygen efficiently at low temperatures (normally 60~120 °C).[15] We should note that previous reports have shown that the formation of Pt-OH beyond 0.8 V is derived not from the interaction of O_2 with Pt, but rather from the reaction of H_2O with Pt, thereby inhibiting O_2 reduction.[16, 17]

In terms of relevant benchmarks, ORR activity is usually expressed in terms of two types of measurements, namely the specific area activity (SA) and the Pt mass activity (MA). In particular, SA possesses a unit of mA/cm^2, indicating a current response that is normalized to surface area, i.e., per cm^2 of catalyst surface, while MA maintains a unit of A/mg_{Pt}, denoting the current normalized to the actual amount of Pt being utilized. The United States Department of Energy (DOE)[18] has proscribed a set of 'benchmark' standards for research purposes, with an MA target of 0.44 A/mg_{Pt} @ 900 $mV_{iR\ free}$ and a corresponding SA target of 0.72 mA/cm^2 @ 0.9 V for electrocatalysts for use in the portable applications market by the year 2017. By comparison, the currently commonly employed commercial catalyst, Etek Pt/C, typically achieves an SA of 0.2 mA/cm^2 and MA of 0.1 A/mg_{Pt}. This reality further supports the notion that electrochemical activity needs to be dramatically and tangibly improved for widespread commercial applicability.

Understanding the precise structure-property correlations between (i) the particle size, shape, and morphology on the one hand and (ii) the intrinsic electrochemical activity, i.e., as manifested in

SA data obtained in a perchloric acid ($HClO_4$) electrolyte, in Pt nanoparticle (NPs) systems used as ORR catalysts has been the subject of intense scrutiny. For example, in early studies, it was discovered that a reduction of mean particle diameter from 15 nm to 3 nm could effectively raise the Pt dispersibility from 5 to 80 m^2/g_{Pt}, thereby increasing the number of available active sites and not surprisingly, leading to a ~5-fold improvement in Pt mass activity.[19, 20]

Furthermore, in the size regime under 3 nm, it has been found that the measured specific activity generally increases with increasing NP diameter. Yet, this relationship is complex, as it has been challenging to find an 'ideal' particle size. For instance, Shao et al.[21] demonstrated that Pt NPs undergo a significant decrease in activity when the diameter was reduced to below 2 nm, while Chorkendorff et al.[22] discovered a volcano-type trend in mass activity with the highest value achieved with particle sizes measuring ~3 nm. Furthermore, it is known that the exposed Pt(111) surface has been found to exhibit the highest activity amongst all of the facets in weakly adsorbed electrolyte, such as the $HClO_4$ electrolyte, thereby rendering octahedral (as well as either tetrahedral or icosahedral) shaped NPs as potentially 'ideal' geometries. A detailed description of all of these prior studies and many others has been provided in a previous Perspective article and in accompanying references.[20] Collectively, these works suggest a need to tweak, optimize, and control the interplay of both the size and the shape of Pt NPs to achieve overall better performances.

However, more recent studies describe alternative scenarios in terms of designing an 'optimized' Pt NP. Specifically, the work of Markovic et al.[23] suggests that as catalysts (especially in the ultrasmall regime of 2 to 7 nm) age, the particle size/shape effect becomes significantly less important, due to the idea of 'morphological evolution'. In particular, after a potential cycling of 4000 cycles (up to 1.1 V), both as-prepared cubic and octahedral NPs evolve into round-like polyhedral shapes, thereby suggesting that particle shapes are inherently difficult to preserve under functional ORR conditions. Consequently, it has been proposed that 7 nm cubo-octahedral Pt NPs represent a

reasonable balance or compromise between (i) the mass activity and (ii) the performance durability (i.e. obtained after 4000 sweeps between 0.6 and 1.1 V at 50 mV/s in a 0.1 M perchloric acid electrolyte environment), which are often competing considerations, as shown in Figure 2.

Meanwhile, it has been observed that particle proximity can also play a decisive effect in influencing catalytic performance.[24] In other words, by deliberately changing the interparticle distance of closely packed assemblies of Pt clusters, the observed catalytic activity was noted to be ~6 times higher than what is observed for commercial Pt NPs and can potentially approach the surface activity expected for bulk Pt. In all, the crucial task in modifying Pt NP-based ORR catalysts recently has been not only to control (i) the size dispersion and corresponding substrate coverage but also to (ii) stabilize the specific shapes of the nanoparticles during the electrochemical reactions themselves.

One major route for improving upon the performance of Pt-based catalysts has been through deliberate modifications in morphology. Specifically, single-crystalline one-dimensional (1D) nanostructures possess (i) high aspect ratios, (ii) fewer lattice boundaries, (iii) long segments of smooth crystal planes, and (iv) a low number of surface defect sites, all of which are desirable attributes for fuel cell catalysts.[25, 26]

By contrast, there are several inherent problems that are associated with 0D NP morphologies. In general, NP morphologies maintain a proportionally larger number of lattice boundaries and defect sites on their surfaces as compared with their 1D-type analogues.[15] Defect sites are less catalytically active than smooth crystal planes, because of local differences in coordination geometry and surface energy, which can change the interface between exposed Pt atoms and the oxygen-rich adsorbate, for instance. Moreover, lattice boundaries and defect sites in NPs can degrade more easily, because these regions display surface Pt atoms with lower coordination numbers, which are more prone to irreversible oxidation. Hence, NPs possess a lower percentage of catalytically active surface area and maintain relatively low stabilities, thereby hindering their long term use. Not surprisingly, the use of 1-

D morphologies, such as nanowires (NWs) and nanotubes (NTs), have been shown by our group and others to lead to inherently better electrocatalytic performance.[27] Hence, structural anisotropy often gives rise to higher intrinsic catalytic activity.

In particular, ultrathin Pt NWs maximize the surface area-to-volume ratio and decrease the amount of catalytically inaccessible material within the interior of the wire, which in turn can generate superior activity as compared with both Pt NTs and NPs.[25] For example, we ourselves have reported on the synthesis, characterization and electrocatalytic performance of ultrathin Pt nanowires with a diameter of less than 2 nm.[27] An acid-wash protocol was employed in order to yield highly exfoliated, crystalline nanowires with a diameter of 1.3 ± 0.4 nm. The electrocatalytic activity of these nanowires toward the oxygen reduction reaction (ORR) was studied in relation to the activity of both supported and unsupported Pt nanoparticles as well as with previously synthesized Pt nanotubes. Our ultrathin, acid-treated, unsupported nanowires displayed an electrochemical surface area activity (ECSA) of 1.45 mA/cm^2, which was nearly four times greater than that of analogous, unsupported platinum nanotubes and seven times greater than that of commercial supported platinum nanoparticles, as shown in Figure 3, panel A~C. Furthermore, Yao et al.[28] fabricated Pt nanowires possessing average diameters of 4 nm through an in situ growth process onto an underlying carbon matrix. According to results from the membrane electrode assembly (MEA) test, the predominantly (111)-oriented facets and relative open access of oxygen to the Pt NW structure contributed to their higher observed performance as compared with that of conventional catalysts.

Most recently, in a more generalized search for viable alternatives to conventional Pt electrocatalysts, our group[29] has also synthesized ultrathin, ternary PtRuFe NWs, possessing different chemical compositions in order to probe their CO tolerance as well as electrochemical activity as a function of composition for companion reactions to ORR, more specifically for both (i) the methanol oxidation reaction (MOR) and (ii) the formic acid oxidation reaction (FAOR). Specifically, as-

prepared ‘multifunctional’ ternary NW catalysts exhibited both higher MOR and FAOR activity as compared with binary Pt_7Ru_3 NW controls, mono-metallic Pt NWs, and commercial catalyst samples. In terms of synthetic novelty, we utilized a sustainably mild, ambient wet-synthesis method never previously applied to the fabrication of crystalline, pure ternary systems in order to fabricate ultrathin, homogeneous alloy PtRuFe NWs with a range of controlled compositions. These NWs were subsequently characterized using a suite of techniques including XRD, TEM, SAED, and EDAX in order to verify not only the incorporation of Ru and Fe into the Pt lattice but also their chemical homogeneity, morphology, as well as physical structure and integrity. Lastly, these NWs were electrochemically tested in order to deduce the appropriateness of conventional explanations such as (i) the bi-functional mechanism as well as (ii) the ligand effect to account for our MOR and FAOR reaction data. In terms of catalytically significant findings, methanol oxidation appeared to be predominantly influenced by the Ru content, whereas formic acid oxidation was primarily impacted by the corresponding Fe content within the ternary metal alloy catalyst itself.

Three-dimensional hollow nanostructures, on the other hand, as compared with their solid counterparts, represent especially promising structural motifs due to many intrinsic attributes including but not limited to a large surface area, a rich surface chemistry, and a relatively low cost of production. It is furthermore crucial that the fabrication of such complex nanostructures also be technically facile and environmentally friendly in scope. In this vein, an aqueous solution-based method relying on galvanic replacement has been developed to yield porous Pt dendritic nanotubes with high crystallinity, outstanding activity, and much greater stability as compared with Pt NPs; these novel nanomaterials are shown in Figure 3D and 3E.[30] Similarly, a one-pot thermal decomposition method, using platinum(IV) complexes as reaction precursors, was utilized to generate a three-dimensional platinum nanochain network (Pt-3NCNW). The highlights of this particular work were (a) the elimination of use of any surfactants and templates as well as (b) the surprising absence of individual, discrete Pt

nanoparticles within the interconnected network itself, whose overall framework may have effectively suppressed the Ostwald ripening effect known to govern the behavior of smaller nanoparticles.[31]

Nevertheless, despite all of these efforts, a reduction in Pt loading is still highly desirable due to the high cost of Pt, as previously discussed in the Introduction. Therefore, complementary approaches towards creating a novel, high performance catalyst have relied on either maximizing Pt usage, significantly reducing the amount of Pt, or yielding a completely Pt-free catalyst. Moreover, it should be noted that under current consumption requirements, there is an insufficient global reserve of Pt to provide for the needs of an effective fuel cell for every car produced. Therefore, it is absolutely necessary in the future to replace platinum either completely or in part with far more plentiful (and cheaper) first row transition metals. Inevitably, in the field of noble-metal based ORR catalysts, these efforts have channeled into the synthesis and production of Pt- and palladium (Pd)–based alloys and core-shell structures as opposed to pure Pt alone. Moreover, noteworthy studies have focused on the generation of classes of non-noble-metal-based and even metal-free catalysts to mitigate for the inherent deficiencies of Pt.

2.2. Survey of Current state-of-the-art technologies

2.2.1. Pt-based catalysts

(A) Pt-metal alloys

One of the most common strategies to reduce the amount of Pt employed in a catalyst is by alloying Pt itself with either another metal or metals. Studies have shown that 3*d* transition metals, such as Mn, Fe, Ni, Co, and Cu, represent potential candidates with which to alloy with Pt.[32] Specifically, platinum-metal-based (i.e. Pt_3M) NP alloys, wherein the metal 'M' can be a subset of (but not necessarily limited to) Ti, V, Fe, Co, Cu, and Ni, with a molar ratio of 3: 1 in favor of Pt, all have exhibited superior ORR specific activities in 0.1 M $HClO_4$ electrolyte as compared with their pure Pt

analogues. The origin behind the observed improvement in activity is believed to be attributed to the downshift of the *d*-band center[33] of the Pt catalyst induced by the presence of the additional 3*d* transition metal(s), thereby leading to a lower coverage of oxygenated species (i.e. OH^-) at normal operating potentials, and thus increasing the number of Pt active sites, accessible to oxygen molecules and protons. This will, in turn, render these oxygenated species present more mobile on the surface, such that they can interact with available protons, and thereby favor the desorption of water molecules. As a result, these alloyed structures do typically exhibit higher ORR activities as compared with commercial Pt NPs.

More recently, (i) controlling the morphology of as-prepared Pt-based metal alloy nanostructures as well as (ii) simplifying synthetic protocols used to create these alloys with the goal of avoiding complicated protocols involving potentially deleterious organic reagents have become primary areas of focus. To address the first issue, it should be noted that manipulating morphology is pivotal in fabricating ORR catalysts that not only possess high activities but also are stable in acidic media. To emphasize the significance of morphology, Yang et al.[34] noted that alloy Cu_3Pt nanoframes are more effective for ORR but are not as useful for MOR by comparison with analogous core-shell Cu-Pt nanoparticles; the core-shell nanoparticles presumably mitigate for the poisoning effect associated with methanol cross-over in direct methanol fuel cells (DMFCs). As another relevant example, a Pt mass activity record of 3.3 A/mg_{Pt} has been observed, by Xia et al., with 9 nm Pt-Ni octahedra, representing over a ten-fold activity improvement as compared with their spherical NP counterparts.[35] In effect, the reported Pt−Ni octahedra gave rise to a 17-fold higher Pt mass activity at 0.9 V along with a ~50-fold improvement in specific activity at 0.93 V, all relative to the behavior of conventional, state-of-the-art Pt/C catalysts, as shown in Figure 4.

To deal with the second concern, the idea of promoting a more facile, more efficient, and sustainable synthesis of Pt alloy-based NPs has also emerged with the intent of raising yields and

improving sample quality, while simultaneously lowering costs. For example, it has been recently reported that nanoporous PtFe structures can be synthesized by merely de-alloying PtFeAl ternary alloys.[36] The key innovation in this work has been the removal of a catalyst support. Indeed, the absence of such a support greatly enhanced the structural stability of nanoporous PtFe alloys as compared with both PtFe/C and Pt/C controls, when analyzing the durability of these materials after electrochemical testing. In a different example,[37] a surfactant-free synthesis approach has been proposed as a means of generating three-dimensional (3D) porous bimetallic alloy nanosponges with (i) a homogeneous size dispersion, (ii) an enhanced electrocatalytic activity, (iii) an excellent stability, and (iv) the possibility for facile large-scale production with a potential for efficient commercialization. All of these studies have unequivocally demonstrated that improving both morphology and synthesis protocols are immensely impactful and significant, when designing novel Pt-based ORR catalysts.

(B) Pt-based core-shell and hierarchical structures

The concept of developing even more sophisticated Pt-based hierarchical structures has materialized and manifested itself in the production of novel core-shell, ternary alloy, hierarchical ternary, and quaternary core-shell structures.[38] Additional complex hierarchical architectures do exist, including but not limited to dendritic, self-assembled-based, and metal@metal oxide structures, respectively. However, core-shell structures represent still the most significant and relevant hierarchical motif.

What are the advantages of a core-shell motif, for example?[33] The core-shell motif itself has three primary benefits toward enhancing the intrinsic activity of electrocatalysts. *First*, a so-called advantageous 'ligand effect', induced by the dopant metal upon the overall catalytic performance, is hypothesized in which the transition metal 'M' core will couple with the external Pt shell, thereby resulting in a beneficial coupled electronic and structural effect, which should increase reaction kinetics. *Second*, it optimizes the use of Pt, thus minimizing Pt loading, and allows for every surface Pt

atom to be catalytically accessible. *Third*, the addition of the transition metal 'M' will lower the energy of the Pt *d*-band and create *d*-band vacancies, thereby enabling a lowered binding energy of oxygen-containing species.

Nevertheless, due to their structural complexity as compared with simple alloys, core-shell structures remain controversial due to potential issues associated with their degradation behavior and corresponding durability. A recent review[38] has sought to summarize these concerns, highlighting the overall importance of the Pt shell thickness, the composition of the core, and the effective particle size in influencing possible degradation and durability under realistic operating conditions.

Therefore, to mitigate for these problems, many recent studies have deliberately sought to optimize morphology. One route involved the use of an annealing process on a Pt_3Co alloy so as to yield a PtCo@Pt core-shell structure with a 2-3 atomic-layer-thick Pt shell.[39] As a result of this Pt shell, these nanoparticles, characterized by a stable ordered core-shell structure, gave rise to a much higher durability with stability tests, evincing a minimal loss of activity even after 5,000 potential cycles. Another reported strategy has sought to utilize gold (Au) as an "interlayer" between a Ni core and a Pt-Ni alloy shell.[40] According to Stamenkovic et al., this complex hierarchical material combined the stabilizing effect of Au with a low-cost core material, i.e. Ni. Based on experimental results, their catalyst exhibited an 8-fold increase in activity as compared with Pt NPs alone. In addition, this core-shell catalyst underwent less than 10% activity loss after 10,000 potential cycles, representing a far better result than what has been previously obtained with comparative structures such as (i) PtNi/C with a multilayered Pt-skin, (ii) Pt/C, and (iii) PtNi/C with Pt-skeleton surfaces, respectively, as illustrated in Figure 5. In essence, this group proved that enhanced ORR activity and durability can be controlled and 'selected for' by simply tailoring the structural motif of their nanomaterials.

2.2.2. Pd-based nanostructures: potential Pt replacement

Palladium (Pd) possesses very similar physical properties to that of Pt, including an *fcc* crystal structure and a similar atomic radius, and yet, it is much less costly than Pt. Moreover, in acidic media, Pd possesses a higher ORR activity than almost any other noble metal, except for Pt. In fact, monometallic Pd nanocatalysts can serve as promising ORR catalysts themselves. For instance, it has been demonstrated that Pd nanocubes enclosed by (100) facets are comparable to Pt nanoparticles in terms of ORR activity.[41] Therefore, not unlike the development of Pt-based catalysts, Pd represents a legitimate building block material and a core design component of ORR catalysts from which subsequent alloy and hierarchical structures have been envisioned and created.

(A) Pd-Pt system

Initially, Pt-Pd alloys were investigated as a promising substitute for Pt itself, since the 'ligand effect' mentioned earlier would account for their superior performance as compared with Pt alone.[42] Not surprisingly, work has focused on creating morphological variants of this bimetallic alloy, including ones based on dendrites, core-shell architectures, and multi-shelled structures. Synthetic approaches used to generate these structural motifs have included but not been limited to the use of co-chemical reduction, galvanic replacement, seed-mediated growth, and a combination of thereof, with the objective of synthesizing Pd–Pt bimetallic nanocrystals with a specific, precise, and well-defined structure. Amongst these different structural motifs, bimetallic nanoparticles either coated with a Pt monolayer or created in the guise of a core-shell architecture have attracted the most attention due to their highly "efficient" Pt loading. However, two major challenges remain to be overcome in order for these materials to be practical and relevant, namely (i) the possibility of synthesis scale up with control over size, shape, and morphology as well as (ii) long-term stability and durability.

As a result, different strategies have been employed to mitigate for both of these issues. For example, Kim et al.[43] developed a one-step synthesis which yields well-defined Pd-Pt core-shell nanoparticles possessing an average size of 5-6 nm. In essence, through a targeted and fortuitous metal

precursor selection, sequential reduction of Pd and Pt ions could be achieved in a straightforward manner within a one-pot environment to generate the desired core-shell objective. In another study that used atomic layer-by-layer deposition to create a quantitatively modifiable Pt skin on Pd nanocubes, Xia et al.[42] were able to infer a direct correlation between the number of Pt monolayers and the corresponding electrochemical durability of these core-shell species. According to their data, Pd nanocubes possessing 2-3 layers of Pt on their outer surface demonstrated the highest mass activity noted of around 0.2 A/mg_{Pt} after 10,000 potential cycles, which is nearly 3-fold higher than that observed with Pt NPs. All of these studies have opened up new and plausible pathways towards designing optimized core-shell Pt-Pd nanostructures.

In our own group, we have reported on the synthesis, characterization, and electrochemical performance of novel, ultrathin Pt monolayer shell ~ Pd nanowire core catalysts.[44] Initially, ultrathin Pd nanowires with diameters of 2.0 ± 0.5 nm were generated and a method has been developed to achieve highly uniform distributions of these catalysts onto the Vulcan XC-72 carbon support. As-prepared wires were activated by the use of two distinctive treatment protocols followed by selective CO adsorption in order to selectively remove undesirable organic residues. Subsequently, the desired nanowire core-Pt monolayer shell motif was reliably achieved by Cu underpotential deposition (UPD) followed by galvanic displacement of the Cu adatoms. The surface area and mass activity of the acid and ozone-treated nanowires were explored and the ozone-treated nanowires were found to maintain outstanding area and mass specific activities of 0.77 mA/cm^2 and 1.83 A/mg_{Pt}, respectively, which were significantly enhanced as compared with conventional commercial Pt nanoparticles, core-shell nanoparticles, and acid-treated nanowires. The ozone-treated nanowires also maintained excellent electrochemical durability under accelerated half-cell testing and it was found that the area-specific activity increased by ~1.5 fold after a simulated catalyst lifetime.

(B) Pd-M system

Historically, enhanced ORR activities have been observed with bulk alloy systems composed of sputtered Pd connected with either Co, Ni, Cu, or Cr in acidic solution. Predictably, many groups have also reported on comparatively encouraging ORR behaviors with analogous Pd-based alloy nanoparticles.[41, 45] In terms of binary alloys, Pd-based systems coupled with 3*d* transition metals such as Co, Fe, and Ni have seemed promising. For instance, alloying Pd with Fe in a 3:1 molar ratio (i.e. Pd_3Fe/C) gave rise to the greatest specific activity observed toward ORR, with a current density of 0.791 mA/cm^2 as compared with 0.131 mA/cm^2 for that associated with Pd/C from Etek, obtained at 0.85 V. Additionally, this Pd_3Fe/C catalyst also achieved a 1.4 fold higher mass activity as compared with Pt/C isolated from Etek at 0.85 V. Similarly, exceptionally good activities, which are comparable to that of Pt, have been recorded with alloys such as but not limited to Pd_4Co[46, 47] and $Pd_{60}Ni_{40}$[48]. In terms of Pd-based ternary alloys, impressive specific activities of up to 4.5 A/m^2 measured at 0.7 V were noted with a Pd: Co: Mo alloy, composed of a molar ratio of 70: 20: 10, representing an improvement of more than 2-fold as compared with a commercial Pt control.

In an effort to further decrease the amount of potentially cost prohibitive metal content such as Pd, the introduction of dopants, such as much cheaper Cu, into functional alloys has been investigated as well.[49] Specifically, Pd-Cu nanoparticles possessing sizes of 5-10 nm and a Pd: Cu molar composition of 1: 1 have shown promising activity, even after a heat treatment at 500ºC. Meanwhile, analogous PdCu nanocubes, possessing a 1: 1 molar ratio of Pd to Cu and characterized by an average diameter of 12 nm, have been found to surpass the ORR activity of corresponding Pd nanoparticles by more than 3-fold.

As for 1-D Pd-M nanostructures, we ourselves have noted similar trends. For instance, in our recent study involving ultrathin (~2 nm) Pd-Ni nanowires, we discovered a volcano-type relationship between chemical composition and ORR activity, which peaked with the formation of Pd_9Ni, though

others had previously reported optimal NP performance with a composition of $Pd_{60}Ni_{40}$.[50] In prior work, it has been demonstrated that the Pd-M alloy tends to undergo Pd segregation in either its uppermost top surface layer or even its several top-most layers. Hence, we attribute this noticeable difference in electrochemical behavior between NWs and NPs to potentially differential degrees of surface segregation and 'islanding' of Pd atoms. In other words, the actual surface composition of previously reported alloy NPs and NWs is likely to be significantly different as compared not only with each other but also with the bulk, and may even vary from the expected overall composition. To further explain and verify this assertion as well as to probe the interplay between the Pd-rich-skin and the Pd-M core, additional theoretical studies will be needed in the future.

Although the electrochemical activities of Pd-based nanoscale alloys have improved significantly over the years, the relatively poor long-term durability of these electrocatalysts in general still remains as a stumbling block, inhibiting future PEM fuel cell applications. One solution to address this issue has been to add in less active metals, such as either Mo or Au,[51-54] though very few reports have specifically examined the long-term stability of these systems.

Another possible strategy has been to deposit a Pt monolayer onto the exterior of these catalysts. For example, our group has recently developed hierarchical 1D nanostructures possessing a Pt-monolayer-shell coupled with a Pd_9Au core.[55] Specifically, initial, as-prepared Pd_9Au NWs maintained significantly enhanced ORR activity (0.40 mA/cm^2), as compared with elemental Pd NW/C (0.12 mA/cm^2) and Pt nanoparticles (NP) /C (0.20 mA/cm^2), respectively. After the deposition of a Pt monolayer, a volcano-type composition dependence was observed in the ORR activity of the $Pt\sim Pd_{1-x}Au_x$ NWs as the Au content is increased from 0 to 30% with the activity of the $Pt\sim Pd_9Au$ NWs (0.98 mA/cm^2, 2.54 A/mg_{Pt}), representing the optimum performance. We noted that the platinum group metal activity of the ultrathin 2 nm NWs (0.64 A/mg) is significantly enhanced as compared with that of analogous 50 nm NWs (0.16 A/mg) and commercial Pt NP/C (0.1 – 0.2 A/mg), thereby highlighting

and reinforcing a distinctive size-dependent enhancement in NW performance. We also found that the structural integrity of the 1D morphology was still well preserved even after a run of 30,000 potential cycles, and furthermore, a slight enhancement in activity was observed, possibly due to a preferential restructuring of the thin, outer Pt monolayer.

2.2.3. Generation of Precious Metal-Free Catalysts

It would obviously be preferable to completely eliminate the presence of any platinum group elements (including Pd) whatsoever, if possible, to achieve the goal of developing cheap, sustainable, and high performance ORR electrocatalysts for PEM fuel cells. Consequently, significant effort has been targeted at designing and optimizing the performance of non-precious metal and metal-free electrocatalysts to rival that of Pt-based catalysts. Examples of potential classes of promising non-Pt catalytic systems include Co- or Fe-based porphyrins and phthalocyanines. These materials incorporate either (i) metal-N_4 (M–N_4) chelates or (ii) 3*d* transition metal complexes linked to N_4 macrocycles.[45] Additionally, these catalysts are generally inert in alcohol, which is an additionally positive and auspicious attribute for their extended applicability in DMFCs. However, these catalysts still require significant additional attention and work, prior to becoming viable alternatives to both Pt- and Pd-based catalysts.

The mechanism of ORR performance in Pt-free, porphyrin-based catalysts is still ill-defined. Though the Fe-N-C site is considered to be mechanistically involved, a detailed understanding of its fundamental role and functionality in ORR remains sadly lacking. Furthermore, this type of catalyst suffers from low stability in acidic media, which is typical of a PEMFC environment. Nonetheless, the durability of porphyrin-based catalysts in acid could be realistically and significantly ameliorated by using either (i) ordered mesoporous porphyrinic carbons (M-OMPC)[56] possessing high surface areas and tunable pore structures or (ii) multi-walled carbon nanotubes (CNTs) in the role of either an underlying template[57] or structural support in order to approach and possibly even surpass the

robustness of Pt/C, in some cases. A relevant example utilizing ordered mesoporous porphyrinic carbons is illustrated in Figure 6. Overall, these reports suggest that the presence of a relatively more stable carbonaceous framework and scaffold might enable porphyrin-based ORR catalysts to survive the harsh, acidic environment characteristic of operational PEMFCs.

In general, nitrogen-doped CNTs (NCNTs) have been found to exhibit promising activity for Pt-free catalysts, due to their unique electronic properties presumably derived from the conjugation between the free lone-pair electrons on the nitrogen and the graphene-like π-conjugated system. By analogy with metal-N-based catalysts, these NCNTs are also susceptible to corrosion resistance in acidic media. However, there have been reports successfully incorporating NCNTs within PEMs. For instance, Dai et al. developed a plasma-etching technology to generate metal-free particle catalysts for the subsequent efficient metal-free growth of CNTs.[58] Interestingly, these metal-free NCNTs evinced relatively good electrocatalytic activity of up to 1.2 mA/cm^2 at 0.2 V vs. an Ag/AgCl reference electrode, as well as long-term stability toward ORR in an acidic medium, as compared with nitrogen-free CNTs. To explain this behavior mechanistically, Terakura et al.[59] noted that only N-derived free lone-pair electron-doped Stone-Wales defect sites appeared to provide for reasonable active sites, so that future studies have concentrated on optimizing the geometry within this precise region.

Moreover, metal oxides, especially the oxides of groups IV and V, can potentially serve as ORR catalysts if their energy levels can be precisely and deliberately tuned.[60] However, it should be noted that in general, metal oxides simply lack sufficient catalytic activity to be competitive with commercial Pt. Nevertheless, the most advantageous property of metal oxides is its high chemical stability towards acids. As a particularly illustrative example, Gebauer et al.[61] utilized a relatively facile combination of sol-gel synthesis and subsequent calcination steps to produce electrocatalysts composed of a series of Pt-free, N/C doped Ti(IV)-oxides. The higher electrocatalytic activity observed with these doped oxides as compared with bare TiO_2 could be attributed to the presence of

both Ti–O–N and Ti–O–C groups. It was found that experimentally defined variables such as the calcination temperature and the N: Ti ratio can have a measurable and marked impact upon electrochemical performance. In effect, the observed ORR activity peaked as compared with an as-prepared TiO_2 reference material, demonstrating a current density of -3.8 $\mu A/cm^2$ at 0.4 V for the Pt-free doped oxide. This novel oxide catalyst was prepared at a calcination temperature of 250ºC, and its structure functionally represents an optimized balance between crystallinity and surface area trends. In addition, it was noted that the N: Ti molar ratio actually gave rise to a monotonic relationship with catalytic activity, as defined by the corresponding increase in active sites.

As a related material, Domen et al.[60] have suggested TaO_x as a promising ORR catalyst candidate. Specifically, TaO_x nanoparticles of various sizes can be prepared by electrodeposition in either nonaqueous $TaCl_5$ or $Ta(OEt)_5$ ethanolic solutions. Based on electrochemical tests, it was determined that the smallest oxide particles (~1 nm in diameter) yielded an onset potential of 0.92 V as well as an ORR activity of 20 mA per g of Ta at 0.6 V. Such size-dependent activity trends are believed to originate from both improved electroconductivity as well as from an increase in available accessible active sites.

2.2.4. Future directions with Catalysts

For the range of Pt- and Pd-based nanostructures we have highlighted herein, it is reasonable to assume that high activity is a necessary but not necessarily sufficient criterion for an effective ORR catalyst; high dispersion and stability are also essential and crucial.[20] A major challenge therefore will be to scale up synthesis without compromising effective control over size, shape, and morphology, especially in the case of a well-defined, high surface-area structure, such as either complex hierarchical or porous materials, which are understandably particularly preferable as ORR catalysts.

Concerning progress in developing non-precious-metal and metal-free catalysts, tangible improvements in the following areas are clearly sought. *First*, it is clear that synthesizing a high-

surface area and stable carbonaceous structural support will be useful. *Second*, it will be critical to more fully create, manipulate, and fundamentally optimize the active sites in these systems. Presumably this will involve a more thorough understanding and correlation of the defects (such as the presence of vacancies and interstitial sites) in these systems with electrochemical properties. *Third*, understanding the exact mechanisms involved with the observed ORR activity in these nanostructures is challenging in terms of explaining how each individual reaction variable precisely correlates with structure and the resulting electrochemical property trends.

Nevertheless, a significant amount of work and effort has been expended towards achieving active non-precious-metal and metal-free catalysts. It has unequivocally been demonstrated that carbon-based nanostructures possessing doping elements, such as either N or transition metals, can be competitive with Pt-based ORR catalysts in terms of yielding outstanding ORR performance, which can presumably be further tuned and optimized by controllably altering the physical and electronic structure of these materials. The real opportunity here will be to create an alternative, cost-effective pathway towards commercialization of portable and stationary FC devices as well as of FCVs.

2.3. Alternative Substrates

As discussed in the previous section, the overall Pt usage can be lowered by creating either alloyed or core-shell Pt-based catalysts. Nonetheless, the fundamental challenge remains as to how to maintain or improve catalyst activity and durability while simultaneously reducing or eliminating Pt loading. Essentially, traditional carbon-supported catalysts suffer from a degradation problem, which is largely affected by temperature, pH, potential, as well as the humidity and purity of the fuel.[62]

As compared with other issues associated with the catalyst material itself, the commercial supporting material, i.e. Vulcan carbon, can be more prone to undergo a destructive disintegration in acidic media. In other words, carbon black (CB) can potentially undergo electrochemical oxidation to surface oxides, and eventually onto CO_2. In fact, catalyst failure can often be attributed to the corrosion

of carbon substrates. Hence, to mitigate for potential degradation effects and the subsequent aggregation of Pt NPs, various other carbonaceous or non-carbonaceous nanomaterials have been introduced as potential catalyst supports.

In particular, as has been previously implied, CNTs are highly regarded as support media for ORR catalysts as a result of a number of desirable attributes, including but not limited to their high surface area, electronic conductivity, as well as their relative stability and corrosion resistance when exposed to an acidic environment. As opposed to raw unprocessed CNTs, surface functionalized CNTs are even more appealing as catalyst supports due to their potential for "anchoring" and favorably influencing the subsequent activity and robustness of immobilized catalyst particles, i.e. Pt nanoparticles.[62] For instance, DFT calculations[63] have predicted that the presence of SH groups on CNTs can not only restrict particle migration but also enhance the oxidative resistance of Pt clusters attached onto CNTs. Specifically, by inhibiting Pt-O and Pt-OH formation, the greater observed stability of this architecture likely emanates from (i) an increased interaction between Pt and SH-CNTs as well as from (ii) a depressed *d*-band center of the Pt NPs.

The extra, nuanced step of adding in conjugated polymers such as polypyrrole (PPy) and polyaniline (PANI) to these CNT systems can lead to the formation of covalent bonds between Pt atoms and polymer-derived N atoms which can prevent sintering of Pt NPs. For instance, in a reported Pt-PANI-MWCNT heterostructure, PANI was found to concentrically wrap around the CNTs, like a sheath, due to bonding between the nanotubes and the polymer.[64] As compared with raw MWCNTs and CB-based counterparts, this more complex hierarchical structure gave rise to high electrochemical activity as well as to excellent electrochemical stability in accelerated degradation tests, as shown in Figure 7. In particular, the specific electrochemical active surface area (ECSA) of Pt/C drops to 40% of its initial value after only 1,400 potential cycles. The analogous benchmark for Pt/CNT is 3,100 cycles.

By contrast, Pt-PANI/CNT can undergo 4,500 cycles before ECSA drops to 40% of the initial value, and remains at 38% of its initial threshold, after 5,800 cycles.

By comparison with CNTs, graphene can also serve as an ORR catalyst support. Due to its low manufacturing cost, reduced graphene oxide (rGO) has become even more popular than graphene itself. For example, a recent theoretical study[65] has shown that in a system composed of Pt_{13} nanoparticles supported onto defective graphene, the O_2 dissociation activation energy was reduced by more than half from 0.37 to 0.16 eV. This effect was likely due to possible charge transfer from Pt atoms to both defective graphene and O_2. Experimentally, Pt nanocubes supported onto rGO[66] can be synthesized via a facile one-pot approach with the resulting Pt product exhibiting enhanced catalytic activity and excellent electrochemical stability by comparison with commercial Pt/CB electrocatalysts.

In addition to graphene-based materials, hollow carbon spheres (HCSs) have also been investigated over the years due to (1) their mesoporous structure, which is conducive to the subsequent uniform dispersion of NPs and (2) their high stability, owing to the underlying, chemically inert graphitic structure. Not surprisingly, Pt/HCS systems have shown greater electrocatalytic stability presumably due to stronger physical interactions between the Pt NPs and the underlying HCS as compared with a standard carbon black support.[67] Moreover, recent research has revealed that nitrogen doping, which was supposed to improve beneficial metal-support interactions, did not necessarily lead to an enhancement in catalyst stability.[68] Structural characterization of nitrogen-doped hollow carbon spheres (NHCS) supported Pt nanoparticles along with an electrochemical comparison between the behavior of nitrogen-doped systems and their non-nitrogen-doped counterparts are illustrated in Figure 8. Indeed, this material is still relatively novel, so further studies are required to systematically understand the nature of the interplay between Pt NPs and HCSs.

By contrast with conventional wisdom which favors the use of electronically conductive materials, i.e. Vulcan carbon or CNTs as PEMFC catalyst substrates, some recent studies have

demonstrated that certain metal oxides are also promising as viable candidates, owing to the 'strong metal support interaction (SMSI)' effect which states that the catalytic behavior of metallic NPs dispersed onto a normally inert metal oxide support can be significantly increased by the underlying oxide support.[69] For instance, the electronic structure of a generic TiO_2 support can be tuned either by adding in oxygen vacancies or by doping with fluorine. The result is that a 70 mV positive shift of the oxygen reaction potential could be achieved for Pt NPs immobilized on this processed, doped support as compared with a corresponding pristine TiO_2 support.[70] Data on other metal-based oxides and support systems, such as SnO_2, indium-doped tin oxide (ITO), SiO_2, and WC, have been summarized in a recent review.[62]

As such, specialized CNTs, graphene, and other types of carbonaceous supports do offer improved durability as compared with conventional CB. Nonetheless, various degrees of carbon corrosion still persist for these functionalized surfaces. Hence, certain metal oxide supports, such as but not limited to TiO_2, SnO_2, SiO_2, Nb_2O_5, RuO_2, offer a positive and plausible substitute, due to their intrinsic resistance in acidic media, yet the ramifications of using these materials for electrocatalysis are still relatively unknown and demand further study and attention. Indeed, one key question that needs to be addressed involves the lack of a comprehensive understanding of the particle-support interaction, which greatly influences the mobility and adhesion of NPs on the support surface. Additionally, detailed systematic investigations (including membrane electrode assembly studies, continuous cycling investigations, and accelerated degradation tests) will still be required in order to understand the behavior of these materials under 'realistic' fuel cell operating conditions.

3. Membranes

A membrane is a material that acts as a barrier, preventing either the transport or mixing of substances from one side to the other. Various types of membranes exist, including cation exchange,

anion exchange, and porous membranes. In particular, anion exchange membranes conduct anions, such as OH^-, whereas cation exchange membranes such as Nafion permit the passage of cations such as H^+. Currently, some limitations exist with anion exchange membranes in alkaline media, including the low stability of OH^- in a less than optimally hydrated membrane, as well as the relatively low conductivity of OH^- as compared with H^+. Additionally, some membranes possess amphoteric dual functionality, i.e. allowing for the transport of both anions and cations due to the presence of both weak acidic and weak basic groups throughout the matrix. As a result, the sign of the charged groups is dependent upon both pH and electrolyte in the bulk solution. Porous membranes, on the other hand, can be tailored so as to selectively allow the gases they are designed and targeted for to diffuse through, based upon their pore size. Depending on the sizes of the pores themselves, it is feasible and possible to trap not only gases but also ions. More specifically, the more porous the membrane, the more dopants can be isolated and captured, including either phosphoric or sulfuric acid, which in turn will presumably increase the proton conductivity of the membrane as a whole. Additionally, rationally selected inorganic filler species can also be 'immobilized' within the porous membrane in order to favorably enhance a particular attribute of that membrane. Nevertheless, the voids within the membrane will only be as large as the targeted molecules ultimately passing through, thereby allowing for efficient gas and ion separation. We focus on proton exchange membranes in our discussion.

Nonetheless, we would like to emphasize our particular focus on sulfonic acid-containing membranes. In particular, the presence of sulfonic acid groups is necessary to improve upon the intrinsic membrane performance, such as its ability to swell. Specifically, the hydrophilic nature of sulfonic acid groups enables water molecules to be retained and kept, even at higher temperatures when membranes tend to dry out, thereby improving overall hydration. Consequently, by tailoring the amount of sulfonic acid groups to an optimal quantity, the overall membrane conductivity can be improved dramatically, since it is directly related to the amount of water present within the membrane.

Therefore, this section will primarily focus on membranes that possess sulfonic acid groups that should enhance their intrinsic properties.

Tangible upgrades in membrane durability and conductivity are necessary prerequisites to the development of durable, robust, and long-lasting PEMFCs for FCV applications. More recently, studies have examined novel means of alleviating proton conductivity and water retention issues through the synthesis of both Nafion/hybrid membranes as well as Nafion alternatives. Due to the vast amount of different types of membranes that have been synthesized and employed, only those involved in most recent studies will be discussed in detail. More comprehensive evaluations of research directions aimed at improving existing PEMFC membranes have been discussed in prior reports.[71-73]

Typically, membranes are evaluated by a number of criteria, including but not limited to proton conductivity (mS/cm), water uptake (%), fuel permeability (cm^2/s), acid content (%), ion exchange capacity (IEC) (meq/g), and storage modulus (MPa). Additionally, when these membranes are employed within a fuel cell set-up in the context of a membrane electrode assembly (MEA), additional means of characterization are utilized including power density (W/cm^2), durability, and current density ($mA/cm^{2)}$. Some of these evaluation criteria and metrics will be discussed below.

3.1. Perfluorosulfonic Acid Ionomer-Based Membranes

The perfluorosulfonic acid (PFSA) ionomer membrane, e.g. Nafion created by Dupont, is the most well known and common membrane incorporated within a proton exchange membrane. Its particular chemical formulation is shown in Figure 9.[73] Nafion possesses an excellent proton conductivity of ~0.10 S/cm, when fully hydrated. However, in practice with a 'normal' operating window under 100°C, commercial Nafion 120 achieves lifetimes of a relatively limited ~50000 hours.[74-76] Proton conductivity, a standard evaluation parameter for membrane performance, is directly influenced by the presence of water molecules. In effect, the degree or extent of hydration is often

denoted by λ, i.e. the number of water molecules per sulfonate group. With an increase in the amount of water molecules present, usually between λ = 5-7, interconnected channels can form, thereby allowing for increased proton conduction pathways throughout the Nafion membrane. At approximately λ ≥ 7, a highly intrinsic network is created with the net proton conductivity, approaching that of bulk water.[71]

Within the standard operating temperature range of 0 to 100°C, water management can become a major issue in that as previously mentioned, water is generated both from inherent FC chemical reactions as well as by the humidification system in order to promote good proton conductivity. As a result, water levels can potentially become too high, thereby flooding and damaging the FC itself. Raising the temperature above 100°C limits unfavorable excess water generation,[72] but has the simultaneous and unfortunate effect of dramatically decreasing water network permeability and therefore, proton conductivity.

Another inherent issue associated with these low temperature membranes is methanol crossover, when utilizing methanol as the main fuel.[74] PFSA membranes typically exhibit a fairly large methanol crossover rate of about 10^{-6} mol/cm^{2}s, which is known to decrease current density performance by approximately 50-100 mA/cm^2. This performance loss has two tangible impacts on the FC, namely (i) a waste of fuel needed for FC operation as well a (ii) lowered energy efficiency and FC performance. Strategies employed to mitigate for this issue include either (i) designing new methanol-resistant membranes or (ii) raising the overall operation temperature, which should speed up the kinetics and thus the overall consumption of methanol, the latter point of which would invariably and ultimately reduce the amount available for crossover.

Moreover, Nafion also suffers from additional issues such as (i) a decreased durability at high temperatures, due to an increase in the electrical resistance within the membrane, thereby resulting in a localized heating and degradation of the membrane, as well as (ii) a decreased conductivity at low RH

conditions, as a result of fewer water molecules present within the membrane itself.[13, 77] Hence, to deal with these issues, efforts have targeted either (i) a chemical modification of the intrinsic PFSA structure or (ii) the synthesis of practical replacements. Specifically, in the first case, recently developed protocols have sought to incorporate functionally relevant materials within existing PFSA membranes to create active hybrids that are presumably more retentive of water at higher temperatures and low RH conditions, while simultaneously being more conductive.

For example, Tiantian and co-workers[78] were able to improve membrane conductivity at low relative humidity by creating a novel Nafion/MIL101 hybrid membrane, wherein MIL101 was a specially designed metal-organic framework, not only characterized by a large surface area and cell volume but also filled with phytic acid, which is known as a primary source of phosphorous storage in plants. Phosphate groups are particularly beneficial for membrane applications due to their high proton conductivity at low humidities, their propitious water retention and hydration capabilities, as well as inherently large charge carrier concentrations. Using thermogravimetric analysis (TGA), it was shown that the composite remained stable to temperatures of up to 300°C, while binding onto an increased amount of water molecules, thereby facilitating good proton conductivity. Of the hybrid membranes tested, Nafion/phytic@MIL-12 exhibited the best proton conductivity with values almost by 11-fold better as compared with pristine Nafion under 10.5% RH conditions (Figure 10). By demonstrating a large enhancement in proton conductivity at such low humidity conditions, i.e. low water content, this study highlighted the importance of using a filler molecule, such as phytic acid, to improve PFSA membrane performance.

In terms of an alternative strategy, another group[79] created a zwitterionic microcapsule (ZMC) based on sulfobetaine to tailor the conductivity and water retention properties of Nafion membranes at low RH values. These zwitterionic microcapsules are composed of poly(sulfobetaine), a well known super hydrophilic and ‘ultralow bio-fouling’ material. An ‘ultralow bio-fouling material’ is a substance

that prevents the build-up of microorganisms and harmful contaminants on wetted surfaces, thereby restricting potentially deleterious amounts to less than 5 ng/cm^2, which in turn would render this membrane as a viable constituent component of microbial fuel cells. As opposed to relying on hydrogen bonding alone, the zwitterionic groups present in the microcapsule end up binding onto water molecules much more strongly due to favorable hydration, as mediated by electrostatically-induced interactions. Moreover, the sulfone groups present in the sulfobetaine are also known to be particularly effective at initiating proton transport.

Not surprisingly, this zwitterionic composite coupled within Nafion evinced a significant increase in water uptake measured at 100% RH as compared with Nafion, which had the practical effect of increasing proton conductivity, due to the presence of an extensive percolated water channel network, thereby allowing for enhanced proton transport. It was also proposed that the resulting composite was more mechanically robust, due in part to the presence of the localized 'water reservoirs' created by the ZMCs within the membrane itself. This composite also experienced greater water retention capacity as compared with standard Nafion, which the authors attributed to two key reasons, namely (i) the presence of a strong electrostatic interaction between water molecules and the zwitterionic groups present therein which complemented existing hydrogen bonding interactions, as well as (ii) the ability of the composite to bind additional water molecules more tightly within its 'coordination sphere'. Predictably, when the composite membrane in particular was probed for its proton conductivity properties under 20% RH, it yielded a ~21-fold increase in value as compared with commercial Nafion over a 90 minute test period.

In essence, significant improvements have been made in both water retention and hydration abilities, thereby affecting proton conductivity, simply by introducing either filler molecules or hydrophilic polymer microcapsules in order to reinforce the primary structural and conductivity characteristics of PFSA membranes. Specifically, many different classes of filler molecules have been

employed to enhance a variety of functional attributes associated with Nafion.[80-82] Nevertheless, one key area of current development has been targeted at devising enhanced alternatives to PFSA membranes themselves.

3.2. Alternative Membranes

3.2.1. Polybenzimidazole-Based Membranes

As a potential Nafion substitute, for example, the polybenzimidazole (PBI) polymer membrane possesses excellent chemical and thermal stability with typical operating temperatures between 100-200°C, as well as an increased tolerance to methanol crossover. Typically, this polymer membrane is dip-coated in phosphoric acid (H_3PO_4) solution as a necessary and unavoidable means of improving its overall proton conductivity characteristics. However, at high acid levels, the H_3PO_4 can leach out, and thereby result in mechanical instability issues associated with the membrane. As a result, it is important to optimize the exact concentration of H_3PO_4 when doping PBI membranes in order to prevent their mechanical degradation. The molecular structure of a PBI membrane itself is defined in Figure 11.[73, 83]

Therefore, in order to improve the mechanical robustness of PBI membranes exposed to increasing concentrations of H_3PO_4 and to therefore negative the effect of acid addition, Prasad et al. employed hydrophobic poly(tetrafluoroethylene) (PTFE) as the underlying backbone material[84] in order to boost the strength and stability of the membrane during normal fuel cell operations. It was noted that during full phosphoric acid doping, neither wrinkling nor obvious mechanical weakening of the PTFE-supported PBI membrane occurred. Additionally, in order to render the PTFE surface slightly more hydrophilic and thus amenable to water molecules, the composite membrane was treated with sodium naphthalene.

Two reference membranes were also tested, including a pristine PBI membrane as well as a widely employed composite membrane of PBI/Nafion tailored with untreated PTFE (uPTFE). These membranes were then tested within a membrane electrode assembly (MEA) configuration in order to test their durability during a rigorous cycling protocol. Specifically, the temperature was repeatedly cycled from 180°C to 30°C every 30 minutes while being held at open circuit voltage (OCV) conditions, similar to the procedure used by Volkswagen. In this particular case, the durability test was run at OCV in order to eliminate other factors, such as either acid leakage or chemical degradation. As a result, by measuring the cell voltage as a function of cell current density, the hybrid composite (PBI/trPTFE) was found to demonstrate a maximum power density of 0.221 W/cm^2 as compared with 0.094 W/cm^2 for the corresponding PBI/Nafion/uPTFE membrane after 48 h, which can be seen in Figure 12. The pristine PBI membrane alone degraded very rapidly. Moreover, scanning electron microscopy (SEM) images obtained after the rigorous electrochemical cycling protocol indicated significantly reduced stress and degradation on the membrane, likely a direct consequence of the use of treated PTFE.

Additionally, as with Nafion itself, the idea of using fillers to improve proton conductivity and to reduce methanol permeability while maintaining high thermal and mechanical stability has manifested itself in several parallel efforts. In one study,[85] $BaZrO_3$, a perovskite nanoparticle, was added in order not only to act as a proton conductor but also to facilitate proton transport, and in turn, increase the kinetics for proton conductivity. Interestingly, an increase in H_3PO_4 retention over time coupled with an increased proton conductivity was observed for the composite membrane, doped with 4 wt. % of $BaZrO_3$, as compared with commercial PBI membranes. The increased proton conductivity of 65 mS/cm at 25°C in dry conditions was attributed to the hygroscopic nature of the perovskite NPs, while the improvement in H_3PO_4 trapping could be ascribed to increased hydrogen bonding interactions. However, with an increase in $BaZrO_3$ doping beyond 4 weight %, a decrease in H_3PO_4

trapping occurred, due to the aggregation of the $BaZrO_3$ particles, and as a result, a reduction in active, available surface area.

Other groups have utilized a variety of other fillers including but not limited to TiO_2, SiO_2, CNTs, graphene, and so on, in order to improve specific properties, such as mechanical stability, proton conductivity, methanol tolerance, and acid leaching. In particular, Jana and co-workers[86] focused their work on understanding the structure-property correlations between their filler molecule, i.e. silica terminated with a long chain amine group, and the underlying PBI membrane in order to determine the precise effect the presence of this specific functional moiety had on the performance of silica and in turn, the membrane, as a whole. As a result, this group observed an increase in mechanical, thermal, and chemical stability as well as an increased retention of phosphoric acid groups as compared with traditional PBI membranes.

Jana et al. noted two specific correlations associated with increasing silica content, namely (i) a decreasing trend in phosphoric acid retention (after 4 wt. % silica was added), which was attributed to increased bonding between silica particles and phosphoric acid groups, as well as (ii) the production of self-assembled clusters of silica particles, which allowed for additional proton hopping sites and thereby improved the overall proton conductivity of the membrane. Specifically, this group addressed a need from the community to gain a basic and fundamental comprehension of the interactions, occurring at the filler-membrane interface, with the expectation that such determinations will lead to a better and more directed understanding as to the choice of fillers for future studies.

3.2.2. Sulfonated Aromatic Membranes

Sulfonated hydrocarbons also signify another viable option to the use of PFSA membranes due to their relatively cheap and facile synthesis as well as their ease of disposal. A variety of sulfonated hydrocarbon alternatives exist with polyphenylsulfone (PPS) as one of the most attractive due to its

high mechanical strength, durability under highly acidic conditions, and relatively low manufacturing cost. However, PPS membranes do exhibit some disadvantages similar to those of Nafion, including the need for increased water uptake to engender efficient proton conductivity, especially at high temperatures. Additionally, PPS membranes are often further sulfonated (sPPS) in order to increase proton conductivity, since the presence of sulfonate groups can improve the observed proton transport, as mentioned earlier. Nevertheless, this process can introduce potential problems and obstacles associated with the reaction time and concentration of sulfonating agents. For example, in the absence of optimization, the use of an overly aggressive 'sulfonation' treatment can result in physical degradation of the membrane, whereas the converse (i.e. an excessively mild protocol) will hinder sufficient sulfonation. A representative formulation of a PPS membrane is noted in Figure 13.[73]

PPS membranes have also been chemically modified with (a) hygroscopic nanoparticles to retain water and reduce fuel permeation as well as with (b) strong acids to promote increased proton transport. For example, a novel nanoscale hybrid membrane fabricated from a sulfonated polyphenyl sulfone (sPPS) / phosphotungstic acid (PWA) / silica membrane composite[87] has been proposed for high temperature PEMFCs. Phosphotungstic acid is considered to be the strongest heteropolyacid (HPA) known,[88] and its presence in this membrane is thought to increase the number of active surface functionalization sites for the transport of protons, thereby increasing the overall proton conductivity measured. The introduction of silica is considered to promote adequate water retention within the membrane, even at low RH conditions.

After testing, the membrane maintained reasonable thermal stability up to ~230°C, as determined by TGA. The water uptake for the hybrid membrane was increased by 6.3% as compared with Nafion alone, an observation attributed to the increased retention properties, associated with silica and PWA. When incorporated into an MEA, this hybrid composite membrane also outperformed its pristine sPPS membrane counterpart at low RH (30%) and 85°C, since the former was found to

achieve a power density of 0.45 W/cm^2 at 0.9 A/cm^2 versus a power density of 0.24 W/cm^2 at 0.53 A/cm^2 at 30% RH and 75°C for the latter. Additionally, the sPPS/PWA/silica hybrid exhibited a current density of 0.750 A/cm^2 at a cell voltage of 0.6 V (85°C, 100% RH), denoting a marked improvement as compared with both the pristine sPPS membrane and recast Nafion, which achieved current densities of 0.405 and 0.38 A/cm^2, respectively. The clear and perceptible performance enhancement as compared with both 'control' membranes was explicitly ascribed to the enhanced water uptake, retention, and proton conducting abilities of the PWA/silica composite as well as to the overall stabilizing interactions with the underlying sPPS matrix.

Another option for replacing Nafion is embodied in work on a sulfonated poly(ether ether ketone) or so-called SPEEK membrane. Its prospective promise arises from the commercial availability and widespread ubiquity of poly(ether ether ketone). Additionally, this polymer possesses constructive and compelling attributes similar to those of aromatic polymers, such as exceptional chemical and thermal stability, good mechanical properties, as well as low cost. The molecular structure of a SPEEK-based membrane is illustrated in Figure 14.[73] However, SPEEK is characterized by a reduced lifetime due to issues of degradation, excessive swelling, and brittleness, especially at higher temperatures.

Hence, in order to counter some of these deleterious issues, cross-linking has often been employed to improve membrane durability. In one such approach,[89] a novel architecture known as PANTS was created by cross-linking and incorporating poly(vinylphosphonic acid) functionalized silica nanotubes of varying aspect ratios into SPEEK; varying the silica-based NT ratio apparently impacted upon the resulting proton conductivity of their composite membrane, as can be observed in Figure 15.

Poly(vinylphosphonic acid) (PVPA) was introduced due to its extensive phosphonic groups, which are known to increase proton conductivity, are not affected as much by moisture, and possess

excellent thermal stability. Silica was brought into the system in order to improve the overall water retention properties of the material, as previously described. All of these distinctive membranes exhibited good thermal stability to ~230°C, highlighting their applicability for high temperature PEMFC operations.

The PANTS-functionalized SPEEK membrane increased water retention by 20% as compared with commercial SPEEK, which was attributed to factors including (i) the void in PANTS allowing for excess water to accumulate, (ii) the hydrophilic shell of the PANTS permitting water absorption, and (iii) the corresponding and advantageous hydrophilic interactions between PANTS and the SPEEK membrane that result in the creation of in situ water channels. With the introduction of PANTS coupled with a systematic increase in the silica NT-based aspect ratio, a noticeable rise (~84%) in proton conductivity was observed at 30°C and 100% RH conditions as compared with conventional commercial SPEEK membranes. Overall, the increase in proton conductivity was attributed to the establishment of a network of interconnected and continuous pathways that could be achieved and generated with these high aspect ratio NTs, thereby allowing for a concomitantly more efficient proton transport. Additionally, these hybrid membranes also exhibited reduced methanol crossover from a value of $4.67 \cdot 10^{-7}$ cm^2/s, associated with a commercial SPEEK membrane, to a more optimal value of $3.66 \cdot 10^{-7}$ cm^2/s for a PANTS-functionalized SPEEK membrane. Increasing the filler content (PANTS) actually inhibited the transport of methanol across the membrane by 'rigidifying', in part, the constituent SPEEK chains.

Polyimides represent yet another plausible alternative to the Nafion standard, particularly due to their favorable thermal and mechanical stability as well as overall durability under a variety of harsh operating conditions including heat and corrosive chemicals. Moreover, polyimides can be sulfonated, thereby improving the overall intrinsic proton conductivity and hydrophilicity of these membranes, as

previously described. The chemical structure of these polymers as well as two plausible routes of sulfonation are highlighted in Figure 16.[73]

Although SPI membranes need to be hydrated in order to exhibit increased proton conductivity and typically swell in humid environments, at the same time, these membranes tend to display relatively small deviations in their properties with increasing temperature. Specifically, these membranes maintain similar values for water uptake and swelling ratios over a wide range, thereby rendering these membranes as potentially advantageous for medium to high-temperature functional PEMFCs. As a result of their chemical consistency and stability, additional work has been directed towards tailoring and potentially enhancing specific properties of these membranes, such as their aforementioned tendency to swell in humid environments.

Zhang and co-workers have sought to account for and alleviate this issue by covalently cross-linking SPI membranes.[90] Cross-linking typically limits water uptake, swelling, and methanol permeability, as well as improves the membrane's overall thermal, mechanical, and chemical stability. Moreover, this group used pendant hydrophobic tetrafluorostyrol groups, such as 1,3-bis(2-trifluoromethyl-4-aminophenoxy)-5-(2,3,5,6-tetrafluoro-4- vinylphenoxy)benzene (6FTFPB), as the means with which to cross-link sulfonated co-polyimides. Indeed, by cross-linking pendant groups as opposed to polymer end groups, it was noted that there was an increased control over the degree of crosslinking as well as an enhancement of mechanical stability. This group ultimately chose SPI-20, a commercial membrane, and varied the degree of subsequent sulfonation (DS) between 60-80 mol% in order to achieve a theoretical IEC range of 1.82 to 2.48 meq. g^{-1}, while maintaining an effective cross-linking density incorporating 6FTFPB at 20%.

Upon cross-linking, the composite membrane was probed using dynamic mechanical analysis (DMA) and differential scanning calorimetry (DSC) analysis in order to determine the effect of its structure upon the observed glass transition temperature. Overall, these two techniques demonstrated

an increase in the temperature range in which the membrane (i.e. cured SPI-20-70) could functionally operate from 232 to ~274°C. An increase in thermal stability was also noted with an initial degradation apparent at 320°C, due to the breakdown of the sulfonic acid groups. Moreover, characterization of the water uptake and swelling ratios of these membranes gave rise to similar trends.

In general, an increase in swelling ratio was observed with increasing temperatures, and could be attributed to the degree of sulfonation. Nevertheless, the cured membranes gave rise to an overall smaller swelling ratio, with the lowest ratio of 6.4 achieved with the cured SPI-20-60 membrane as opposed to a ratio of 9 for an uncured, control membrane, all measured at 80°C. In effect, the cured membranes maintained lower swelling ratios as a result of the presence of geometric cross-linking. Furthermore, it was noted that the water uptake in these membranes correlated with a higher degree of sulfonation, an observation which could be ascribed to their intrinsic hydrophilic nature. Not surprisingly, the more highly rigidified and more heavily cross-linked cured samples yielded a lower overall water uptake percentage as compared with their uncured counterparts. Specifically, the cured SPI-20 series gave rise to reduced swelling as a result of the presence of the cross-linking network. We should note that all membranes analyzed (with the exception of SPI-20-80) demonstrated a reduced swelling ratio and water uptake at 80°C as compared with Nafion 117 alone. The associated IEC values dramatically improved for the fully hydrated state of these cured membranes as compared with their uncured analogues.

3.2.3. Phosphonic-Based Membranes

Phosphonic acid-based membranes are highly advantageous for high temperature PEMFCs, due to their amphoteric character, rendering them as suitable candidates not only for high temperature but also for low relative humidity environments. These phosphonic acid groups enhance proton conductivity without necessarily resulting in large membrane swelling, and thereby improve the

mechanical stability of the membrane during cycling. Additionally, phosphonic acid groups are known to possess overall better thermal stability as compared with sulfuric acid groups.[91] An additional example associated with the incorporation of phosphonic acid groups to a SPEEK membrane can be found in section 3.2.2.

In particular, one group, Bigarre et al.[91] demonstrated the wisdom of including phosphonic acid groups within their membrane. Specifically, this group blended a membrane composed of polyvinylidene difluoride and chlorotrifluoroethylene (i.e. poly(VDF-coCTFE)), an inert phase notable for its mechanical and thermal stability, with covalently cross-linked phosphonated polyelectrolytes, which favor an enhanced proton transfer, in order to synthesize semi-inter-penetrated networks (SIPN). This group sought to correlate variations in cross-linking ratios not only with proton conductivity but also with overall mechanical properties.

For instance, this group developed MX-Y, where X corresponds to the mol% of 4-(vinyloxy)butyl methanesulfonate (VBMS) and Y refers to the wt% of poly[(CTFE-alt-DEVEP)-co-(CTFE-alt-VBMS)] with DEVEP representing diethyl vinyl ether phosphonate. When this group subsequently analyzed the proton conductivity of their membranes, they found that at 20°C, the proton conductivity of their test M-100 membrane was ~20 mS cm^{-1} while at 80°C, it was ~1 mS cm^{-1}, a decrease which was attributed to a loss of swelling in the membrane. The cross-linked membranes analyzed (M_5-80, M_{10}-80, and M_{20}-80) evinced an increase in proton conductivity as a function of increasing temperature, an observation which could be ascribed to a more robust membrane structure as a result of the increased cross-linking. However, they also found that their cross-linked membranes do not perform as well as the blended membranes, a fact which could be attributed to (i) the decreased mobility of the phosphonic acid groups as a result of the cross-linking reaction, and (ii) the difference between the macroscopic organization between the blend and the cross-linked membranes.

The group then moved on to analyze the effect of the phosphonic acid groups on the resulting mechanical stability of the membranes. In essence, the mechanical studies performed on the polymers exhibited two trends. (i) When the RH is low, the presence of a high degree of phosphonated terpolymer indicates a high storage modulus as a result of the increased rigidity of the membrane, and hence, the overall mechanical properties are dictated by the phosphonated terpolymer. By contrast, (ii) at high RH, the mechanical behavior is determined by the presence of poly(VDF-co-CTFE), which is associated with a lower storage modulus. Ultimately, this group concluded that during cycling, the degree of mechanical stability will remain relatively high as a result of these overall trends.

3.2.4. Polyphosphazene-Based Membranes

A separate but related alternative is associated with polyphosphazene-based membranes. Polyphosphazene membranes are composed of alternating nitrogen and phosphorous atoms comprising a robust backbone structure, with various types of potential side groups, i.e. organic, inorganic, or organometallic moieties, attached onto the phosphorous atoms, as can be seen in Figure 17.[73]

These membranes exhibit various types of functionalities, which are dependent upon the chemical nature of the specific side groups. However, the backbone itself provides for high torsional mobility as well as stability against free-radical cleavage reactions, thereby rendering these types of membranes as significantly appealing for PEMFC applications. Additionally, these materials are cost effective, non-flammable, extremely hydrophilic due to the presence of the phosphorous atoms, and highly resistant to harsh operating conditions, due to the fact that both the phosphorous and nitrogen atoms are already in their highest oxidation states. These membranes should also be beneficial as components of direct methanol fuel cells, due to their high methanol selectivity. Specifically, linear and cross-linked sulfonated polyphosphazenes exhibit diffusion coefficients, which are two orders of magnitude less as compared with Nafion for water and methanol diffusivity. A more comprehensive

description of this type of membrane has been previously put forth,[73] and we highlight a relevant example herein.

Specifically, one group, Bhat and co-workers,[81] created a blend between a polyphosphazene membrane and a SPEEK membrane in order to beneficially bolster the mechanical strength, oxidative resistance, and chemical tailorability of the resulting composite. This group systematically analyzed the mechanical and thermal strength of the SPEEK membrane as a result of blending in discrete amounts of polyphosphazene. Using thermogravimetric analysis and differential thermogravimetric analysis (DTG), the group determined that upon introduction of polyphosphazene, (i) the weight loss of SPEEK at 300°C was reduced from 20% to 15%, while (ii) its overall thermal degradability shifted to higher temperatures, i.e. from 530°C to 556°C. Moreover, as seen in Figure 12, with increasing amounts of polyphosphazene, the tensile strength increased from 12 to 17 MPa with merely a 3 weight % addition. However, the elongation at the breaking point decreased with increasing polyphosphazene content, which was attributed to the restricted SPEEK chain mobility as a result of the introduction of a polyphosphazene derivative, specifically poly[bis(phenoxy)phosphazene] (POP), which can be seen in Figure 18.

Due to the high methanol selectivity of polyphosphazene , the blended membrane was tested in an MEA configuration under actual DMFC operational conditions. As compared with a commercial Nafion standard, which generated a power density of 47 mW/cm^2, the composite membrane evinced a higher power density, an observation which was attributed to the low methanol crossover and better electrochemical selectivity of this modified membrane. Overall, significant enhancements could be achieved (i) by either employing polyphosphazene membranes and subsequently tailoring their side groups or (ii) by combining these membranes with alternatives such as SPEEK in order to create and/or optimize existing membrane characteristics.

3.2.5. Polystyrene –Based Membranes

Polystyrene sulfonic acid (PSSA) membranes had been the first commercialized PEMFC membrane in 1955 and were used for the Gemini space program. However, this membrane possessed a very limited lifetime of <200 hrs under realistic fuel cell conditions; this was likely due to membrane degradation. With the development of Nafion and its significantly increased lifetime, this specific membrane was overlooked. However, with the recent need to develop effective and functional high temperature membranes, interest in these structures has experienced an unexpected resurgence. Additionally, due to the inherently low cost of polystyrene and hence of styrene-containing membranes as well as to the relatively low methanol permeability of this material, PSSA membranes have been considered as a viable replacement for Nafion in PEMFCs as well as in DMFCs.

However, PSSA membranes are unable to withstand the normal operating conditions within a PEMFC for long periods, leading to losses in both IEC and proton conductivity as well as to deleterious membrane degradation. Specifically, these membranes are destroyed by high peroxide-induced reactivity at various 'weak points' within their chemical structure, for example at the ternary benzylic hydrogen and aromatic ring protons shown in Figure 19.[73] Hence, much research has focused on improving the chemical integrity of PSSA membranes, such as the substitution of various, less reactive side chains or by the addition of 'reinforcing', strengthening functionalities.

For example, Figueiredo et al.[92] enhanced the mechanical stability of their composite membrane at temperatures of up to 140°C by incorporating in bacterial cellulose (BC) as an additive. This strategy led to the development of unique, higher performing PSSA membranes with distinctive advantages over commercial Nafion. Specifically, the group cross-linked PSSA polyelectrolyte within a bacterial cellulose network by utilizing poly(ethylene glycol) diacrylate (PEGDA) as the crosslinking agent. As previously implied, PSSA membranes are attractive, because of their high protonic conductivity, low cost, and sustainable method of synthesis. Typically, PSSA is limited to use in low

temperature PEMFCs, due to its potential for irreversible decomposition at higher temperatures; however, by stabilizing the material with BC, an increase in both the mechanical strength and stability up to 140°C was observed. Moreover, the IEC, which is directly related to the amount of sulfonic acid groups present, was found to increase with increasing amount of the PEGDA cross-linker and therefore, the corresponding quantity of PSSA, which was retained within the BC network.

Ultimately, this group probed the mechanical stability of the composite membrane, composed of a ratio of BC: PSSA: PEGDA of 1: 5: 0.4. This sample along with the 'control samples', i.e. Nafion and pure BC, gave rise to a storage modulus minima (E') at 0°C due to the plasticizing effect attributed to the presence of water; this type of behavior is illustrated in Figure 20. It was found that the composite membrane evinced a E' value of 2.65 GPa at 75°C, which is approximately 20 times higher than that of Nafion, and that this remained constant between 60- ~140°C, due in large measure to the stabilizing influence of the added BC network. A decrease was noted for E' between -10 - 60°C, presumably due to the larger water uptake as well as to the lower fraction of stable BC within the composite itself. At ~160°C and beyond, thermal degradation of the membrane was observed. As a result, this group was able to demonstrate the favorable effect of cross-linking PSSA membranes with a bacterial cellulose network via PEGDA in order to improve the mechanical stability over a large temperature range as compared with both Nafion and bare PSSA membranes. Additionally, they report that this is the first biologically-based PFSA membrane alternative, thereby opening the possibility for cheaper and potentially more efficient membranes for fuel cell applications, based on the use of biological additives.

Additionally, styrene-based monomers represent the most utilized vinyl monomeric unit that can be considered as a grafting monomer for the production of PEMs, not only due to their large supply but also as a result of the exposed benzene rings that can 'host' ionic groups. Grafting is a technique wherein new properties are imparted onto a membrane without either changing or otherwise

influencing the membrane's inherent properties. This procedure allows for a variety of functional groups of different interesting types and modalities to be added onto a membrane in a controlled and quantifiably deterministic fashion. Additional information about various types of grafting techniques and strategies can be found in the following reference.[93]

Therefore, styrene-based membranes enhanced by grafting can be selectively tuned to provide for a variety of favorable properties, as was noted by Nahm et al.[94] Specifically, this group created a poly(styrene sulfonic acid)-grafted poly(vinylidene fluoride-co-hexafluoropropylene) / tin oxide composite membrane, otherwise denoted as PVdF-HFP-SnO_2. SnO_2 was employed as an inorganic filler in order to substantively enhance the specific properties of the composite membrane. In essence, SnO_2 particles are known to increase the thermal stability as well as the water absorption capabilities of membranes. Additionally, SnO_2 particles possess conductivities of $10^{-3} – 10^{-2}$ S/cm at elevated RHs and temperatures, denoting desirable attributes which further validate their usage.

This group determined that the IEC values of the composite membranes were directly proportional to the degree of grafting. In essence, it was found that the greater degree of grafting present, the more sulfonic acid groups were incorporated, thereby directly affecting the water retention capability of the membrane. This membrane characteristic was inversely proportional to the amount of SnO_2 incorporated; that is, the larger the amount of SnO_2 present in the membrane, the lower the level of grating and hence, the less incorporation of sulfonic acid groups. As a result, this group achieved IEC values within the range of 0.68 – 1.15 mmol g^{-1} (i.e. 12 - 3 wt. % of SnO_2). Furthermore, an increase in ion conductivity was also observed with a higher level of grafting. The presence of additional sulfonic acid groups can potentially generate a larger quantity of ion channels and therefore enable more ion migration, thereby ultimately improving ionic conductivity. Furthermore, by not only as a result of the presence of sulfonic acid groups incorporated by grafting but also taking into account of the increased amount of water molecules absorbed by SnO_2 as well as the inherently high methanol

resistance of SnO_2, which was shown to decrease the methanol permeability of the membrane, this group observed an increase in the direct methanol fuel cell performance of their composite membrane, which ended up being comparable to that of a commercial analogue.

3.3. Future Directions with Membranes

The development of improved membranes with enhanced performance will continue to be a primary area of endeavor with which to render fuel cells less expensive and more efficient. The key objective will be to maximize their proton conductivity, water uptake, durability, and mechanical strength as well as to decrease methanol permeability in order to synthesize and assemble an optimized membrane structure. Hybrid membranes therefore represent a particularly promising route forward, since a specific designated functional additive can be incorporated within an existing polymer backbone in order to address a particular problem of concern, associated with membrane inefficiency under high temperature conditions.

Additionally, with the growing push towards the use of fuel cells for transportation applications, the current vehicle market is turning towards DMFCs as a result of current issues associated with hydrogen storage. Therefore, there is an overall need for the generation of methanol-tolerant membranes possessing low methanol permeability. As such, it may be advantageous to enhance and tune membrane properties based upon the specific requirements and needs of the transportation market, i.e. a membrane that can function over a large temperature range under a variety of harsh fuel cell conditions, with reduced swelling and low fuel cross-over. Hence, the idea of cross-linking for example to improve membrane durability and chemical stability represents a promising step forward.

Ultimately, the prevailing thematic undercurrent in these studies will be to more fully understand structure-property correlations in these types of systems. A number of potential avenues of investigation come to mind. For instance, what would constitute an optimal ‘filler’? What happens

when these membranes are reduced in size to a nanoscale level?[95] Moreover, can production of nanoscale membrane materials be effectively scaled up?[96] Can a 'perfect' membrane be designed, essentially *a priori*, on the basis of theory alone and if so, can it be subsequently brought to fruition by careful, directed synthesis? As a result of improved understanding in all of these key areas, membranes can be further optimized for effective use in transportation applications.

4. Conclusions and Overall Future Directions

In this Review, we have sought to probe illustrative examples highlighting the most recent and complementary intellectual currents and directions defining novel catalyst and membrane design, respectively. Currently, Pt-based catalysts still represent the most widely used catalysts for applications in PEMFCs due to their high activity. While efforts towards optimizing (1) the intrinsic particle size of Pt nanoparticles, (2) the production of novel morphological motifs, such as either nanowires or three-dimensional nanostructures, as well as (3) the spatial distribution and dispersion of these nanoparticles onto an underlying support material have been the collective focus of past research, current innovation has transcended the traditional view of elemental Pt itself as the most important and best performing ORR catalyst. Moreover, as previously noted, the highest electrochemical activity reported has been obtained by deliberately tuning the morphology of Pt-based bimetallic nanostructures; in so doing, activities of over a magnitude higher than the state-of-the-art commercial Pt catalyst have been achieved. However, bimetallic Pt-M nanoparticles suffer from considerable losses in performance under realistic fuel cell operating conditions, as a result of degradation issues including but not limited to dissolution of the transition metal itself as well as re-deposition of dissolved Pt.[97] To transcend these limitations, both tri- and multi-metallic nanomaterials, such as either PtPdCo nanoalloy or Pt-shell, bimetallic-core heterostructures, represent promising structural avenues for the development of the

next generation of functional ORR catalyst candidates, yet generalized, large-scale, reliable, and sustainable approaches to reproducibly generating such structures are still lacking.

As for precious metal-free catalysts, despite their respective advantages, i.e., low cost for porphyrin-based materials or high chemical stability in acids for metal oxide-based structures for example, they currently lack sufficient catalytic activity in order to be fully competitive with Pt-containing catalysts. Consequently, all of the aforementioned issues affecting performance will need to be resolved so as to enable FC commercialization. Moreover, a transition away from commonly employed, conventional CB and Vulcan carbon supports to a more ubiquitous use of CNTs, rGO, and metal oxides as underlying substrates should mitigate to some extent for deleterious issues associated with catalytic degradation and agglomeration.

Moreover, it is evident that chemistry plays a large role in creating the next generation of functional architectures aimed at optimizing structure-property correlations in order to overcome existing performance, cost, and durability issues. Specifically, recent work on tailoring membranes for high temperature PEMFCs is focused on modifying the composition of the membranes, such as through the inclusion and addition of either PTFE, phosphate groups, or additives such as PANTS to control for problems associated with proton conductivity, durability, methanol permeability, and mechanical stability. Conversely, advances in catalyst design are targeted towards either minimizing Pt content or creating Pt-less structures in order to synthesize commercially attractive, cost-effective catalysts without sacrificing on activity, durability, and surface area. This goal is further complicated by the need to develop and design a facile, sustainable, and scalable synthesis methodology using either inexpensive metals or non-toxic precursors.

Furthermore, it would be highly beneficial to gain a deeper understanding of the physicochemical nature of the interface between the catalyst and substrate as well as between the membrane and the additive. The ultimate goal is to enhance understanding and to further advances in

proton exchange membrane (PEM) technology beyond that of what is currently employed for commercial (primarily transport) applications. With this objective in mind, complementary computational studies will allow for the possibility of rationally designing new materials for membranes and catalysts as well as novel combinations of such materials with overall superior properties such as higher durability, good performance metrics (including conductivity), and long-term stability. Moreover, advanced *in situ* characterization techniques can provide for a unique, dynamic, and potentially localized understanding of how these particular materials alter, change, and behave, especially under realistic operating conditions.

5. **Acknowledgements**

Research funding for all authors was provided by the U.S. Department of Energy, Basic Energy Sciences, Materials Sciences and Engineering Division, related to our studies, writing, and analyses conducted at Brookhaven National Laboratory, which is supported by the U.S. Department of Energy under Contract No. DE-AC02-98CH10886 and DE-SC00112704. We thank Christopher Koenigsmann for helpful comments and feedback.

References

1. I. Navigant Consulting, *Stationary Fuel Cells; Fuel Cells for Prime Power, Large CHP, Residential CHP, and UPS Applications: Global Market Analysis and Forecasts*, Navigant Consulting, Inc, 2014.
2. S. Satyapal, *U.S. Department of Energy Fuel Cell Activities: Progress and Future Directions*, U.S. Department of Energy, 2012.
3. *2012 Fuel Cell Technologies Market Report*, U.S. Department of Energy 2013.
4. Z. Rao and S. Wang, *Renewable and Sustainable Energy Reviews*, 2011, **15**, 4554-4571.
5. K. Darrow, R. Tidball, J. Wang and A. Hampson, *Catalog of CHP Technologies*, U.S. Environmental Protection Agency; Combined Heat and Power Partnership, 2014.
6. C. Song, *Catalysis Today*, 2002, **77**, 17-49.
7. J. K. Norskov, J. Rossmeisl, A. Logadottir, L. Lindqvist, J. R. Kitchin, T. Bligaard and H. Jonsson, *J Phys Chem B*, 2004, **108**, 17886-17892.
8. W. Vielstich, A. Lamm and H. A. Gasteiger, *Handbook of fuel cells : fundamentals, technology, and applications*, Wiley, Chichester, England ; Hoboken, N.J., 2003.
9. C. He, S. Desai, G. Brown and S. Bollepalli, *The Electrochemical Society Interface*, 2005, **14**, 41-44.
10. J. Zhang, *PEM fuel cell electrocatalysts and catalyst layers : fundamentals and applications*, Springer, London, 2008.
11. *Toyota Unveils Prototype Fuel Cell Vehicle*, Fuel Cell Today, Fuel Cell Today, 2013.
12. M. M. Bomgardner, *Chemical & Engineering News*, 2014, **92**, 17-20.
13. K. Galoustov, M. Anthonisen, D. H. Ryan and D. D. MacNeil, *Journal of Power Sources*, 2011, **196**, 6893-6897.
14. H. Zhang and P. K. Shen, *Chemical Reviews*, 2012, **112**, 2780-2832.
15. *Fuel Cell Catalysis: A Surface Science Approach*, John Wiley and Sons, Hoboken, NJ, 2009.
16. V. S. Murthi, R. C. Urian and S. Mukerjee, *J Phys Chem B*, 2004, **108**, 11011-11023.
17. Y. Xu and B. Zhang, *Chem Soc Rev*, 2014, **43**, 2439-2450.
18. *Fuel Cell Technologies: Multi-Year Research, Development, and Demonstration Plan*, U.S. Department of Energy, 2012.
19. H. A. Gasteiger, S. S. Kocha, B. Sompalli and F. T. Wagner, *Appl Catal B-Environ*, 2005, **56**, 9-35.
20. I. E. L. Stephens, A. S. Bondarenko, U. Gronbjerg, J. Rossmeisl and I. Chorkendorff, *Energ Environ Sci*, 2012, **5**, 6744-6762.
21. M. H. Shao, A. Peles and K. Shoemaker, *Nano Lett*, 2011, **11**, 3714-3719.
22. F. J. Perez-Alonso, D. N. McCarthy, A. Nierhoff, P. Hernandez-Fernandez, C. Strebel, I. E. L. Stephens, J. H. Nielsen and I. Chorkendorff, *Angew Chem Int Edit*, 2012, **51**, 4641-4643.
23. D. Li, C. Wang, D. S. Strmcnik, D. V. Tripkovic, X. Sun, Y. Kang, M. Chi, J. D. Snyder, D. van der Vliet, Y. Tsai, V. R. Stamenkovic, S. Sun and N. M. Markovic, *Energ Environ Sci*, 2014, **7**, 4061-4069.
24. M. Nesselberger, M. Roefzaad, R. F. Hamou, P. U. Biedermann, F. F. Schweinberger, S. Kunz, K. Schloegl, G. K. H. Wiberg, S. Ashton, U. Heiz, K. J. J. Mayrhofer and M. Arenz, *Nat Mater*, 2013, **12**, 919-924.
25. C. Koenigsmann, M. E. Scofield, H. Q. Liu and S. S. Wong, *Journal of Physical Chemistry Letters*, 2012, **3**, 3385-3398.
26. C. Koenigsmann and S. S. Wong, *Energ Environ Sci*, 2011, **4**, 1161-1176.
27. C. Koenigsmann, W. P. Zhou, R. R. Adzic, E. Sutter and S. S. Wong, *Nano Lett*, 2010, **10**, 2806-2811.

28. X. Y. Yao, K. H. Su, S. Sui, L. W. Mao, A. He, J. L. Zhang and S. F. Du, *Int. J. Hydrogen Energy*, 2013, **38**, 12374-12378.
29. M. E. Scofield, C. Koenigsmann, L. Wang, H. Liu and S. S. Wong, *Energ Environ Sci*, 2015, **8**, 350-363.
30. G. X. Zhang, S. H. Sun, M. Cai, Y. Zhang, R. Y. Li and X. L. Sun, *Sci Rep-Uk*, 2013, **3**, 1-8.
31. J. F. Xu, G. T. Fu, Y. W. Tang, Y. M. Zhou, Y. Chen and T. H. Lu, *J Mater Chem*, 2012, **22**, 13585-13590.
32. J. Greeley, I. E. L. Stephens, A. S. Bondarenko, T. P. Johansson, H. A. Hansen, T. F. Jaramillo, J. Rossmeisl, I. Chorkendorff and J. K. Norskov, *Nat Chem*, 2009, **1**, 552-556.
33. J. R. Kitchin, J. K. Norskov, M. A. Barteau and J. G. Chen, *Phys Rev Lett*, 2004, **93**, 156801/156801-156801/156804.
34. L. Han, H. Liu, P. L. Cui, Z. J. Peng, S. J. Zhang and J. Yang, *Sci Rep-Uk*, 2014, **4**.
35. S. I. Choi, S. F. Xie, M. H. Shao, J. H. Odell, N. Lu, H. C. Peng, L. Protsailo, S. Guerrero, J. H. Park, X. H. Xia, J. G. Wang, M. J. Kim and Y. N. Xia, *Nano Lett*, 2013, **13**, 3420-3425.
36. H. M. Duan, Q. Hao and C. X. Xu, *J Power Sources*, 2014, **269**, 589-596.
37. Z. Zhu, Y. Zhai and S. Dong, *ACS Appl. Mater. Interfaces*, 2014, **6**, 16721-16726.
38. M. Oezaslan, F. Hasche and P. Strasser, *Journal of Physical Chemistry Letters*, 2013, **4**, 3273-3291.
39. D. L. Wang, H. L. L. Xin, R. Hovden, H. S. Wang, Y. C. Yu, D. A. Muller, F. J. DiSalvo and H. D. Abruna, *Nat Mater*, 2013, **12**, 81-87.
40. Y. Kang, J. Snyder, M. Chi, D. Li, K. L. More, N. M. Markovic and V. R. Stamenkovic, *Nano Lett*, 2014, **14**, 6361-6367.
41. M. Shao, *J Power Sources*, 2011, **196**, 2433-2444.
42. S. F. Xie, S. I. Choi, N. Lu, L. T. Roling, J. A. Herron, L. Zhang, J. Park, J. G. Wang, M. J. Kim, Z. X. Xie, M. Mavrikakis and Y. N. Xia, *Nano Lett*, 2014, **14**, 3570-3576.
43. Y. Lim, S. K. Kim, S. C. Lee, J. Choi, K. S. Nahm, S. J. Yoo and P. Kim, *Nanoscale*, 2014, **6**, 4038-4042.
44. C. Koenigsmann, A. C. Santulli, K. P. Gong, M. B. Vukmirovic, W. P. Zhou, E. Sutter, S. S. Wong and R. R. Adzic, *J Am Chem Soc*, 2011, **133**, 9783-9795.
45. A. Morozan, B. Jousselme and S. Palacin, *Energ Environ Sci*, 2011, **4**, 1238-1254.
46. H. Liu and A. Manthiram, *Energ Environ Sci*, 2009, **2**, 124-132.
47. B. I. Kharisov, O. V. Kharissova and U. Ortiz Méndez, *Handbook of less-common nanostructures*, CRC Press, Boca Raton, FL, 2012.
48. K. Lee, O. Savadogo, A. Ishihara, S. Mitsushima, N. Kamiya and K. Ota, *J Electrochem Soc*, 2006, **153**, A20-A24.
49. Z. Yin, L. Lin and D. Ma, *Catal. Sci. Tech.*, 2014, **4**, 4116-4128.
50. H. Q. Liu, C. Koenigsmann, R. R. Adzic and S. S. Wong, *Acs Catal*, 2014, **4**, 2544-2555.
51. V. Raghuveer, A. Manthiram and A. J. Bard, *J Phys Chem B*, 2005, **109**, 22909-22912.
52. A. Sarkar, A. V. Murugan and A. Manthiram, *J Phys Chem C*, 2008, **112**, 12037-12043.
53. P. S. Ruvinsky, S. N. Pronkin, V. I. Zaikovskii, P. Bernhardt and E. R. Savinova, *Phys Chem Chem Phys*, 2008, **10**, 6665-6676.
54. J. H. Shim, J. Kim, C. Lee and Y. Lee, *Chem Mater*, 2011, **23**, 4694-4700.
55. C. Koenigsmann, E. Sutter, R. R. Adzic and S. S. Wong, *J Phys Chem C*, 2012, **116**, 15297-15306.
56. J. Y. Cheon, T. Kim, Y. Choi, H. Y. Jeong, M. G. Kim, Y. J. Sa, J. Kim, Z. Lee, T. H. Yang, K. Kwon, O. Terasaki, G. G. Park, R. R. Adzic and S. H. Joo, *Sci Rep-Uk*, 2013, **3**, 1-8.
57. I. Hijazi, T. Bourgeteau, R. Cornut, A. Morozan, A. Filoramo, J. Leroy, V. Derycke, B. Jousselme and S. Campidelli, *J Am Chem Soc*, 2014, **136**, 6348-6354.

58. D. S. Yu, Q. Zhang and L. M. Dai, *J Am Chem Soc*, 2010, **132**, 15127-15129.
59. G.-L. Chai, Z. Hou, D.-J. Shu, T. Ikeda and K. Terakura, *J Am Chem Soc*, 2014, **136**, 13629-13640.
60. J. Seo, D. Cha, K. Takanabe, J. Kubota and K. Domen, *Phys Chem Chem Phys*, 2014, **16**, 895-898.
61. C. Gebauer, J. Fischer, M. Wassner, T. Diemant, J. Bansmann, N. Hüsing and R. J. Behm, *Electrochim. Acta*, 2014, **146**, 335-345.
62. S. Sharma and B. G. Pollet, *J Power Sources*, 2012, **208**, 96-119.
63. L. Li, C. Chen, Z. D. Wei, X. Q. Qi, M. R. Xia and Y. Q. Wang, *Phys. Chem. Chem. Phys.*, 2012, **14**, 16581-16587.
64. D. P. He, C. Zeng, C. Xu, N. C. Cheng, H. G. Li, S. C. Mu and M. Pan, *Langmuir*, 2011, **27**, 5582-5588.
65. D. H. Lim and J. Wilcox, *J Phys Chem C*, 2012, **116**, 3653-3660.
66. B. Y. Xia, H. Bin Wu, Y. Yan, H. B. Wang and X. Wang, *Small*, 2014, **10**, 2336-2339.
67. Z. X. Yan, J. M. Xie, S. K. Zong, M. M. Zhang, Q. Sun and M. Chen, *Electrochim Acta*, 2013, **109**, 256-261.
68. C. Galeano, J. C. Meier, M. Soorholtz, H. Bongard, C. Baldizzone, K. J. J. Mayrhofer and F. Schüth, *Acs Catalysis*, 2014, 3856-3868.
69. S. J. Tauster, S. C. Fung and R. L. Garten, *J Am Chem Soc*, 1978, **100**, 170-175.
70. F. F. Shi, L. R. Baker, A. Hervier, G. A. Somorjai and K. Komvopoulos, *Nano Lett*, 2013, **13**, 4469-4474.
71. H. W. Zhang and P. K. Shen, *Chemical Reviews*, 2012, **112**, 2780-2832.
72. Y. Shao, G. Yin, Z. Wang and Y. Gao, *J Power Sources*, 2007, **167**, 235-242.
73. A. Kraytsberg and Y. Ein-Eli, *Energy & Fuels*, 2014, **28**, 7303-7330.
74. Q. Li, R. He, J. O. Jensen and N. J. Bjerrum, *Chem. Mater.*, 2003, **15**, 4896-4915.
75. O. Savadogo, *J. New Mater. Electrochem. Syst.*, 1998, **1**, 47-66.
76. S. M. J. Zaidi, *Research Trends in Polymer Electrolyte Membranes for PEMFC*, Springer Science + Business Media, LLC, 2009.
77. M. A. Hickner, H. Ghassemi, Y. S. Kim, B. R. Einsla and J. E. McGrath, *Chemical Reviews*, 2004, **104**, 4587-4612.
78. Z. Li, G. He, B. Zhang, Y. Cao, H. Wu, Z. Jiang and Z. Tiantian, *ACS Applied Materials & Interfaces*, 2014, **6**, 9799-9807.
79. G. He, Z. Li, Y. Li, Z. Li, H. Wu, X. Yang and Z. Jiang, *ACS Appl. Mater. Interfaces*, 2014, **6**, 5362-5366.
80. C.-H. Tsai, C.-C. Wang, C.-Y. Chang, C.-H. Lin and Y. W. Chen-Yang, *International Journal of Hydrogen Energy*, 2014, **39**, 15696-15705.
81. S. G. Peera, S. Meenakshi, K. H. Gopi, S. D. Bhat, P. Sridhar and S. Pitchumani, *RSC Advances*, 2013, **3**, 14048-14056.
82. R. Wang, X. Yan, X. Wu, G. He, L. Du, Z. Hu and M. Tan, *Journal of Polymer Science Part B: Polymer Physics*, 2014, **52**, 1107-1117.
83. J. A. Asensio, E. M. Sanchez and P. Gomez-Romero, *Chem Soc Rev*, 2010, **39**, 3210-3239.
84. J. Park, L. Wang, S. G. Advani and A. K. Prasad, *Electrochim. Acta*, 2014, **120**, 30-38.
85. K. Hooshyari, M. Javanbakht, A. Shabanikia and M. Enhessari, *J Power Sources*, 2014.
86. S. Singha and T. Jana, *ACS Appl. Mater. Interfaces*, 2014.
87. Y. Devrim, *Electrochim. Acta*, 2014, **146**, 741-751.
88. T. Okuhara and M. Misono, *Oxide catalysts in solid state chemistry*, John Wiley and Sons, 1994.

89. G. He, L. Nie, X. Han, H. Dong, Y. Li, H. Wu, X. He, J. Hu and Z. Jiang, *Journal of Power Sources*, 2014, **259**, 203-212.
90. H. Yao, P. Feng, P. Liu, B. Liu, Y. Zhang, S. Guan and Z. Jiang, *Polymer Chemistry*, 2015.
91. E. Labalme, G. David, J. Souquet, P. Buvat and J. Bigarre, *Journal of Materials Chemistry A*, 2014, **2**, 9792-9802.
92. T. D. O. Gadim, A. G. P. R. Figueiredo, N. C. Rosero-Navarro, C. Vilela, J. A. F. Gamelas, A. Barros-Timmons, C. P. Neto, A. J. D. Silvestre, C. S. R. Freire and F. M. L. Figueiredo, *ACS Applied Materials & Interfaces*, 2014, **6**, 7864-7875.
93. M. M. Nasef, *Chemical Reviews*, 2014, **114**, 12278-12329.
94. G. Gnana kumar, J. Shin, Y.-C. Nho, I. s. Hwang, G. Fei, A. R. Kim and K. S. Nahm, *Journal of Membrane Science*, 2010, **350**, 92-100.
95. K. A. Page, A. Kusoglu, C. M. Stafford, S. Kim, R. J. Kline and A. Z. Weber, *Nano Lett.*, 2014, **14**, 2299-2304.
96. F. J. Pinar, P. Canizares, M. A. Rodrigo, D. Úbeda and J. Lobato, *J Power Sources*, 2015, **274**, 177-185.
97. J. B. Wu and H. Yang, *Acc. Chem. Res.*, 2013, **46**, 1848-1857.

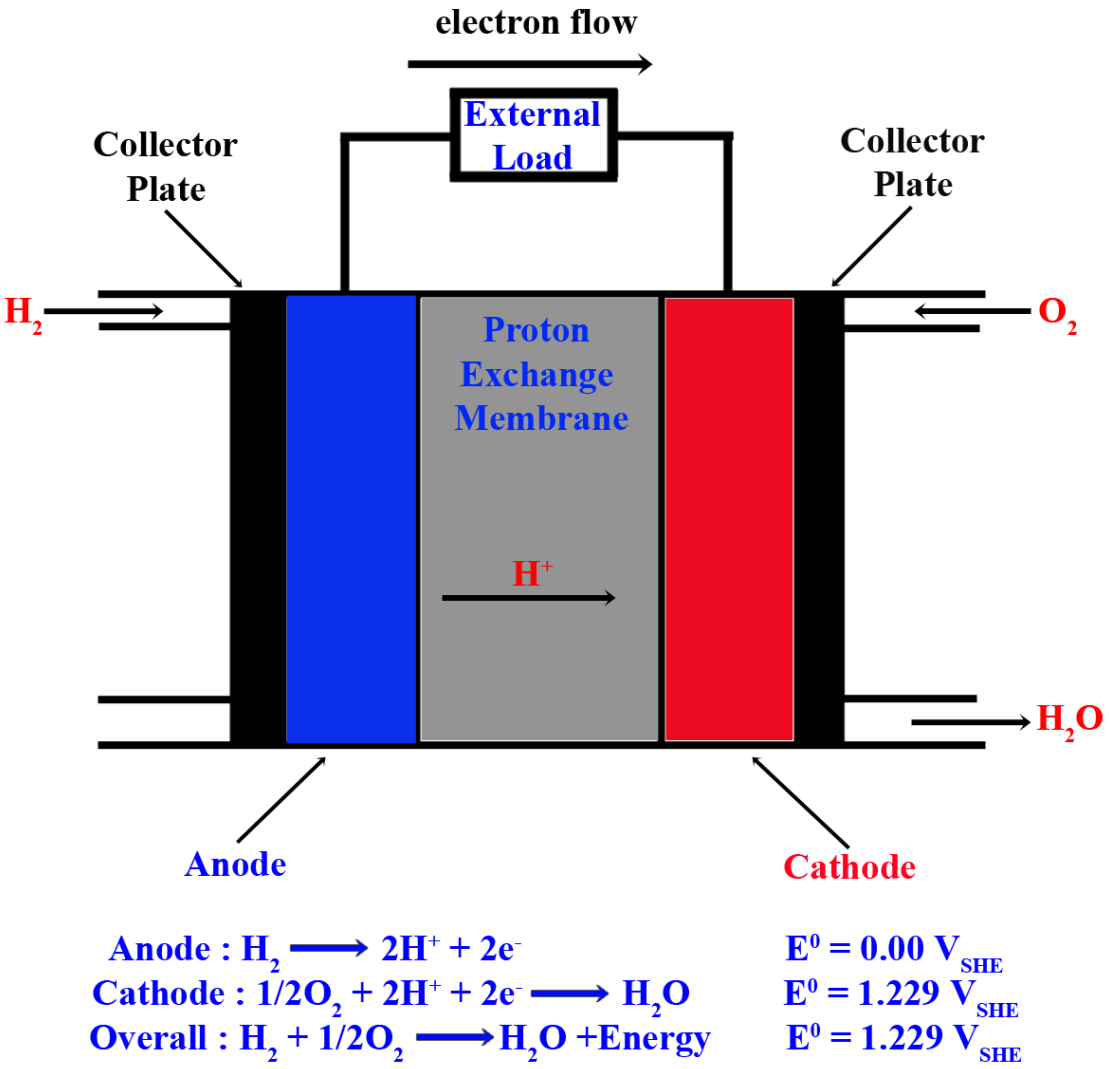

Figure 1. Schematic diagram of a conventional proton exchange membrane fuel cell membrane electrode assembly. Equations pertaining to each half-cell and the overall reaction as well as their standard potentials are noted below the image.

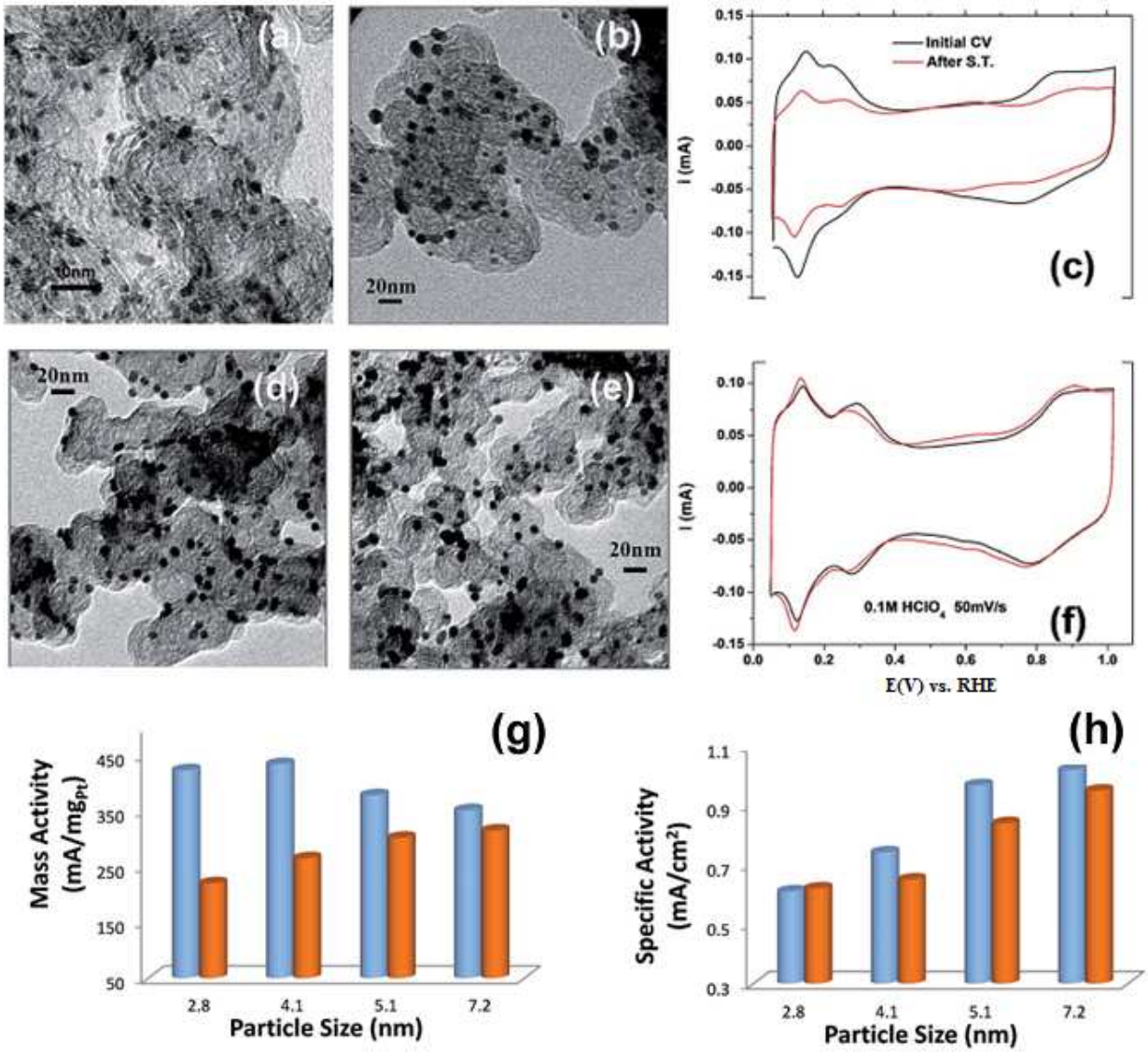

Figure 2. TEM images for the 2.8 nm Pt NPs on a carbon support (a) before and (b) after stability test. (c) Cyclic voltammograms of 2.8 nm Pt/C NPs before (black curve) and after (red curve) stability test. TEM images of 7.2 nm Pt NPs on carbon support (d) before and (e) after stability test. (f) Cyclic voltammograms of 7.2 nm Pt/C NPs before (black curve) and after (red curve) stability test. Summarized mass activity (g) and specific area activity (h) data of different sized NPs before (blue bar) and after (red bar) stability test. Reprinted from reference 23 with permission from The Royal Society of Chemistry.

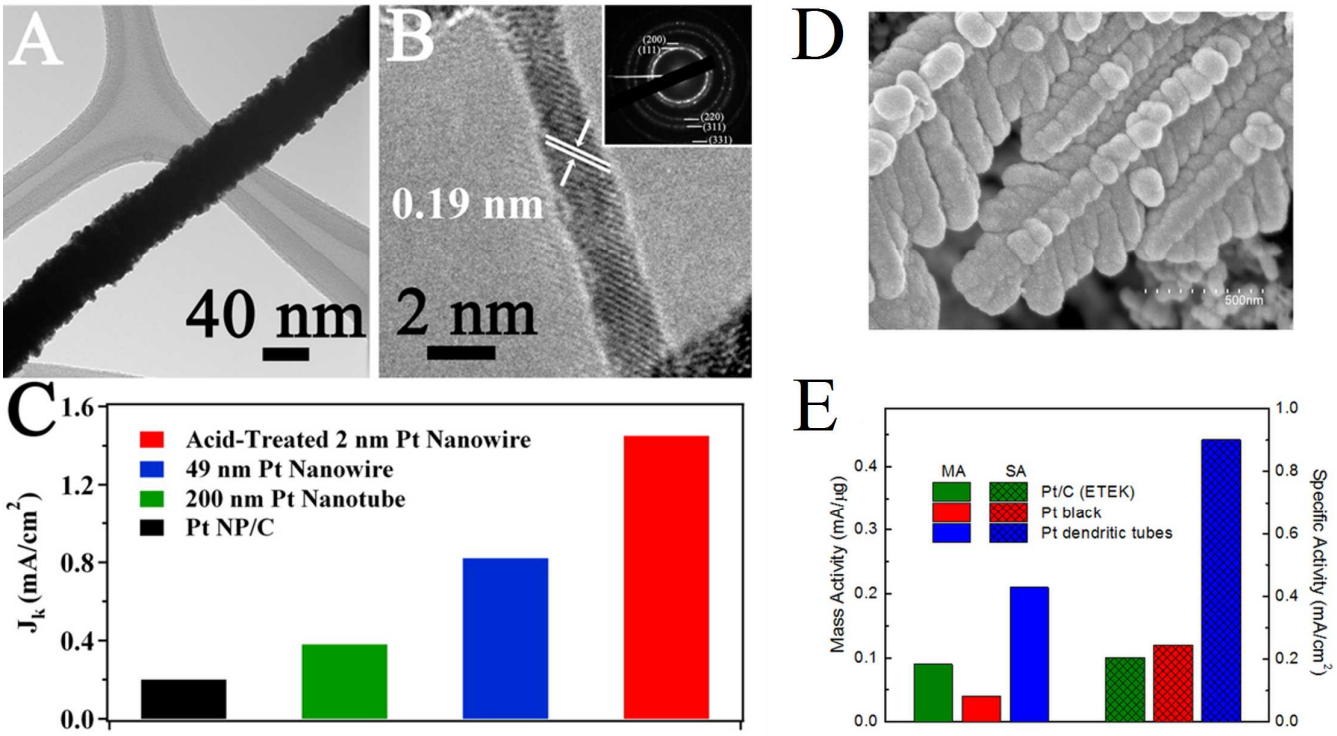

Figure 3. Examples of 1D (nanowires) and 3D (nanodendritic) Pt electrocatalysts and their corresponding performance. Left hand side: representative TEM images collected from individual isolated Pt NWs, possessing diameters of 49 (A) and 2 nm (B), respectively. A representative selected area electron diffraction pattern collected from an ensemble of individual 2 nm NWs is shown as an inset of (B). The size-dependent trend in 1D Pt nanostructures of specific ORR activity measured at 0.9 V with commercial Pt NP/C serving as a commercial reference system is illustrated in (C). Right hand side: SEM images of porous dendritic Pt nanotubes (D) as well as the corresponding mass activity and specific activity measured at 0.9 V (vs. RHE) with commercial Pt/C and Pt black, serving as controls (E). (A)-(C). Reprinted with permission from reference 27. Copyright 2010 American Chemical Society. (D) and (E). Reprinted with permission from reference 30. Copyright 2013 Nature Publishing Group.

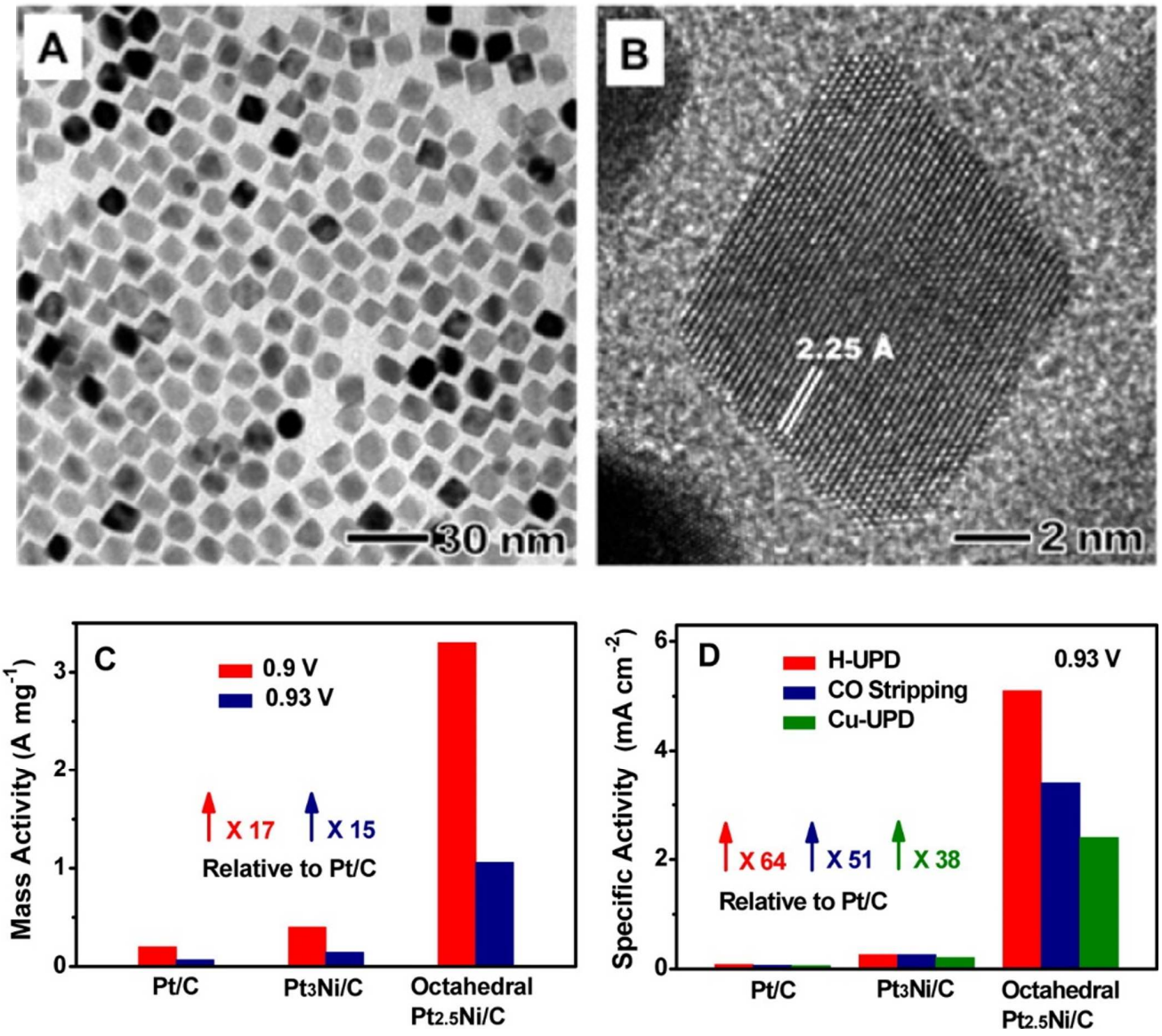

Figure 4. (A) TEM and (B) HRTEM images of as-obtained Pt−Ni octahedra with 9 nm edge length. (C) Comparison of Pt mass activity of Pt/C (TKK), Pt_3Ni/C (TKK), and octahedral $Pt_{2.5}Ni$/C at 0.9 and 0.93 V. (D) Comparison of specific activity at 0.93 V, based on the ESAs, calculated from the charges associated with H_{UPD}, CO stripping, and Cu_{UPD}. Reproduced with permission from reference 35. Copyright 2013 American Chemical Society.

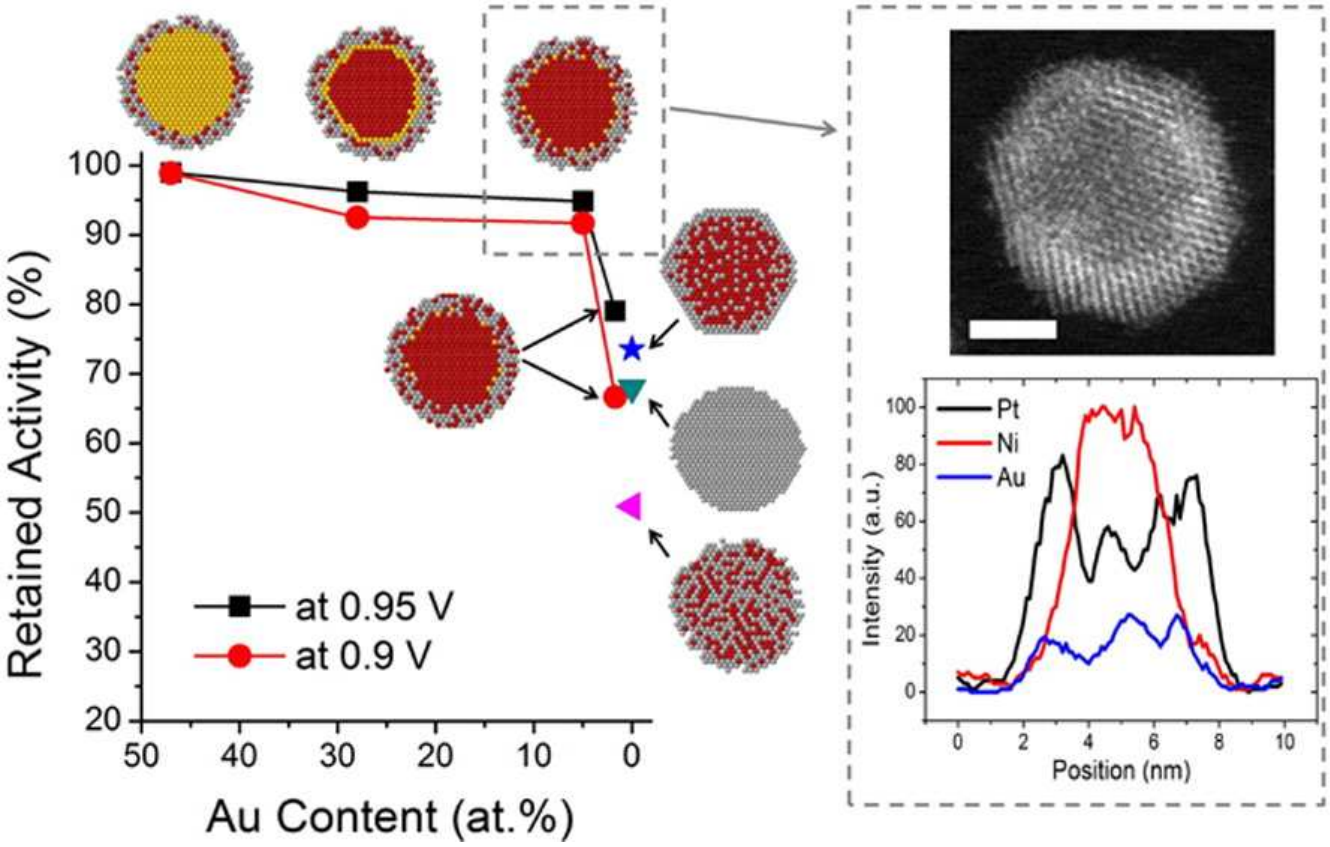

Figure 5. Lefthand side: Correlation between durability (retained activity after 10 000 electrochemical cycles between 0.6 and 1.1 V) and the Au content in the sub-surface of nanoparticles. The activities of the corresponding Pt-Au-Ni nanostructures are presented as the kinetic current densities measured at both 0.95 V (black square) and 0.9 V (red circle). Blue stars, cyan triangles, and magenta triangles represent the retained activity (measured at 0.95 V) of PtNi/C with a multilayered Pt-skin, Pt/C, and PtNi/C with Pt −skeleton surface morphology, respectively. Righthand side: Electron Microscopy of 5.0 nm (σ = 6%) Ni@Au@PtNi nanoparticles, which possess the optimized ORR electrocatalytic performance. Specifically, the dark-field STEM images (top) as well as EDX data (bottom) highlight the core−shell structure of the electrocatalyst. Reprinted with permission from reference 40. Copyright 2014 American Chemical Society.

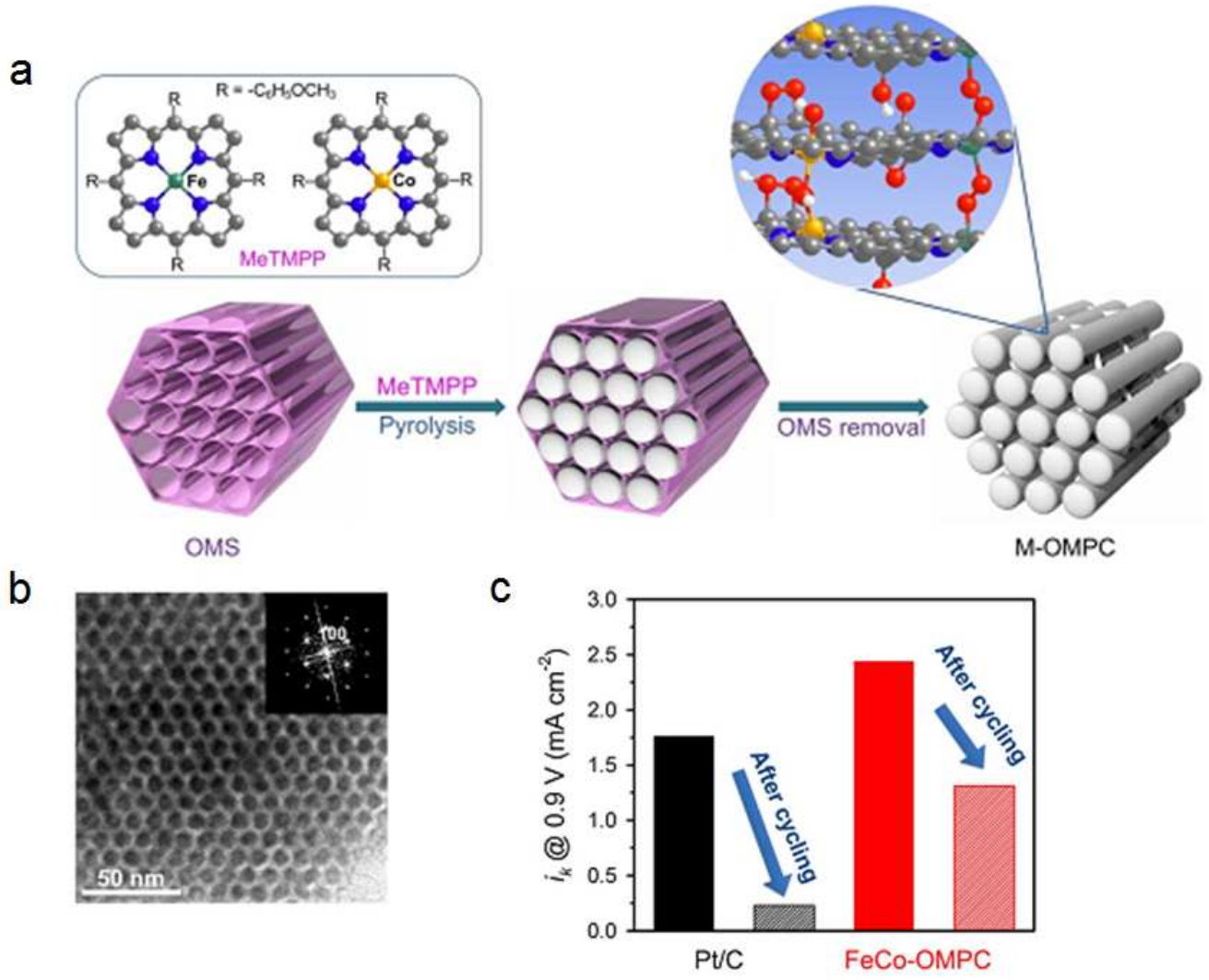

Figure 6. (a) Schematic synthetic strategy of metal incorporated-ordered mesoporous porphyrinic carbons (M-OMPC). The M-OMPC catalysts were synthesized via a nanocasting method that employed ordered mesoporous silica (OMSs) as templates and metalloporphyrins as the carbon source. The high temperature pyrolysis resulted in an OMS/carbon composite, after which the final M-OMPC catalysts were generated through the removal of the OMS template by HF etching. Grey, blue, green, orange, red, and white spheres represent C, N, Fe, Co, O, and H, respectively. (b) TEM image and the corresponding Fourier diffractogram (inset) of FeCo-OMPC showing hexagonal arrays of uniform carbon nanorods and mesopores generated between the nanorods. (c) Comparison of kinetic currents of Pt/C and FeCo-OMPC catalysts before and after 10,000 potential cycles. Reprinted with permission from reference 56. Copyright 2013 Nature Publishing Group.

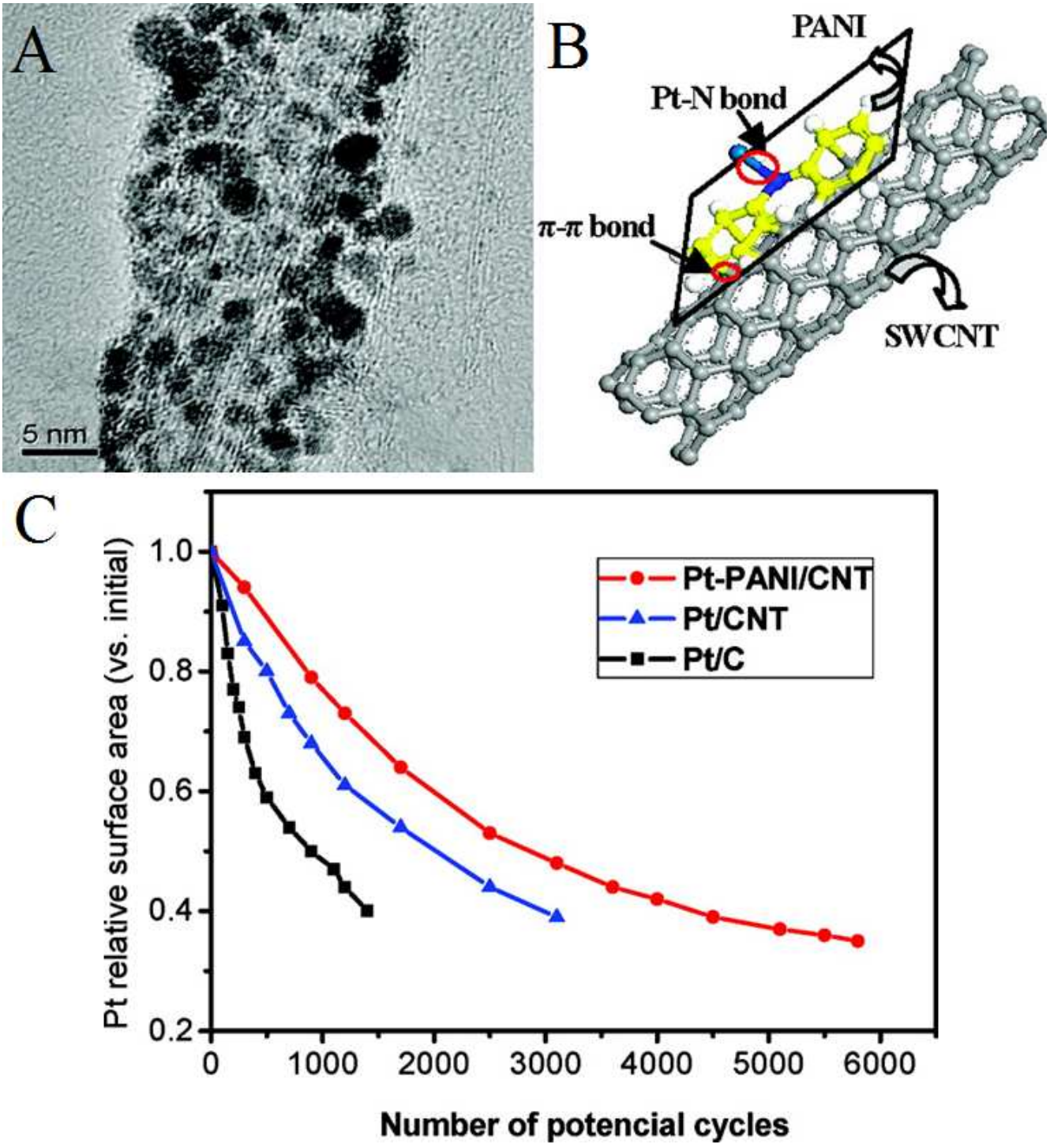

Figure 7. (A) TEM image of 20 wt % Pt-PANI/CNT heterostructure catalysts; (B) Schematic of the molecular interactions in the synthesized Pt-PANI/CNT catalyst; (C) Comparison of electrochemical active area (ECA) of Pt-based catalysts with different substrates including carbon black, unfunctionalized carbon nanotubes, and carbon nanotubes functionalized with polyaniline (PANI), respectively, as a function of the number of potential cycles. Reprinted with permission from reference 64. Copyright 2011 American Chemical Society.

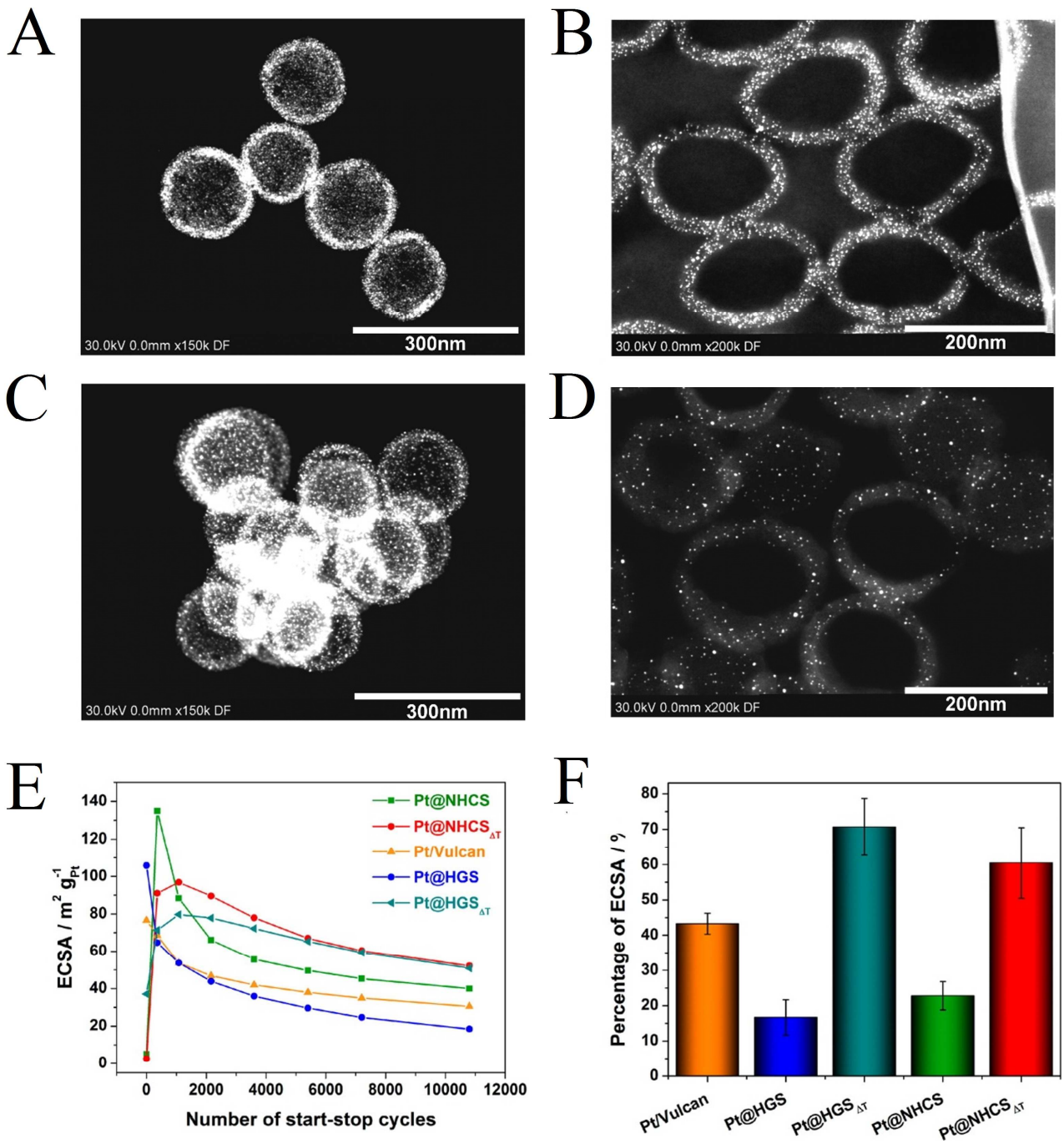

Figure 8. Dark Field-STEM (A,C), and Dark Field-STEM micrographs of cross sections (B,D) of Pt@NHCS as-made (A and B) and Pt@NHCS$_{\Delta T}$ after thermal treatment at 850 °C (C and D). Comparison of the electrochemical properties of NHCS-, HGS-, and Vulcan-based electrocatalysts determined in 0.1 M $HClO_4$. (E) Comparison of ECSA change as monitored via CO-stripping during the ex-situ accelerated degradation test for each catalyst, with degradation cycles between 0.4 and 1.4V RHE at 1 V s^{-1}. (F) Comparison of remaining ECSA as compared with ECSA (initial or after activation) in % after 10800 degradation cycles. Reproduced with permission from reference 68. Copyright 2014 American Chemical Society.

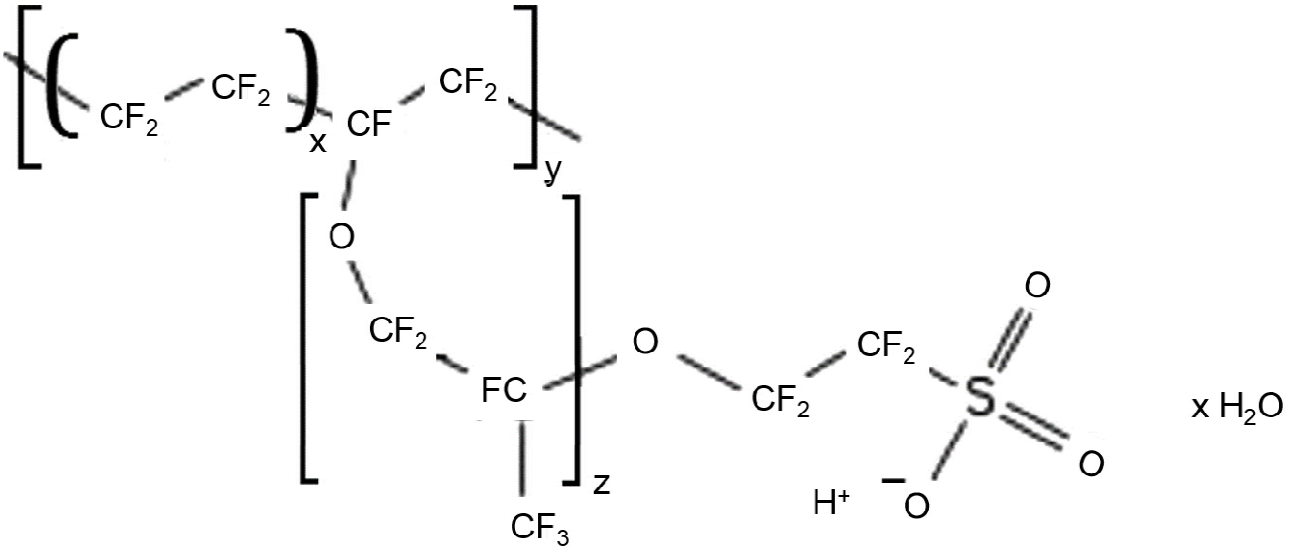

Figure 9. Chemical structure of Nafion. Adapted with permission from reference 73. Copyright 2014 American Chemical Society.

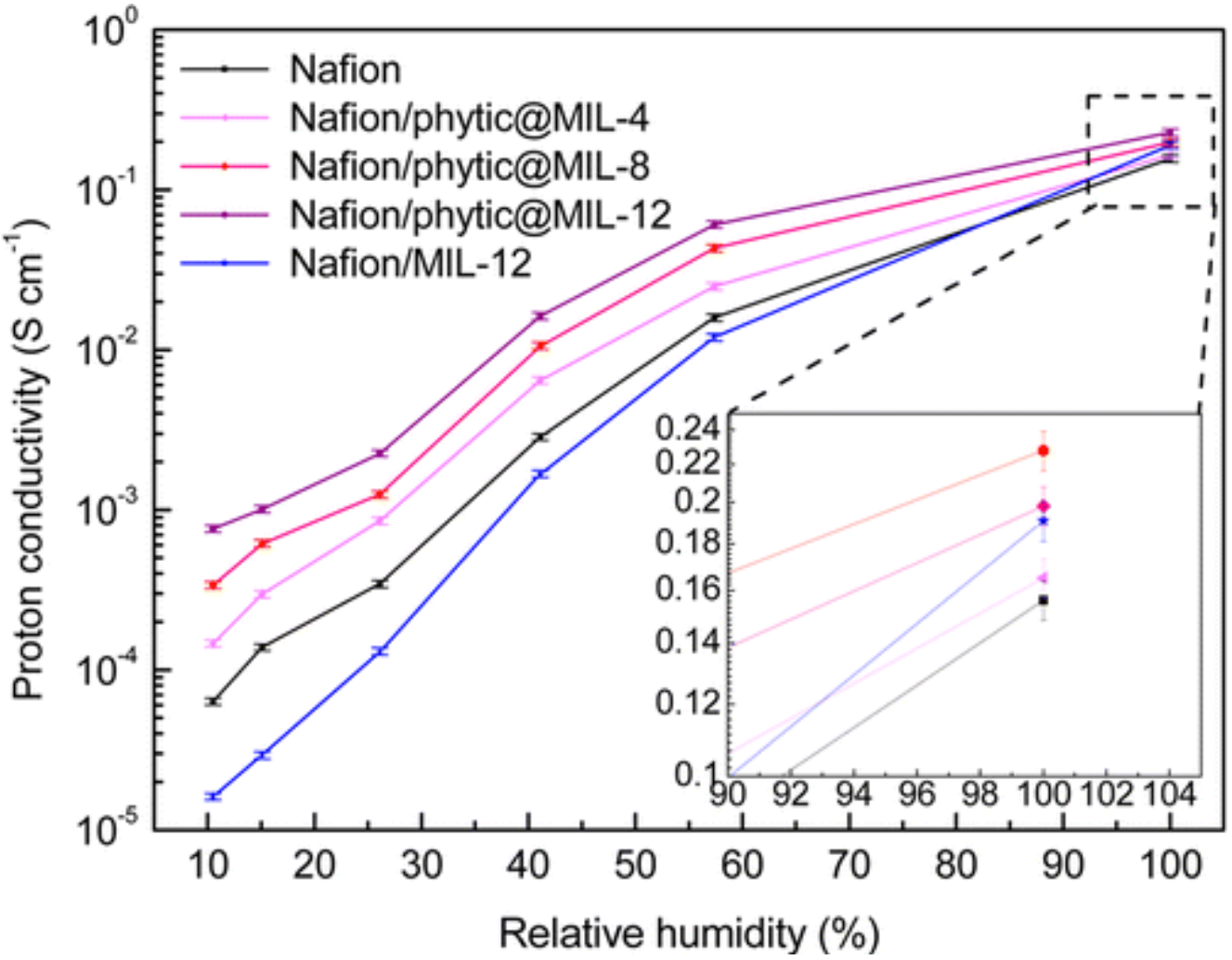

Figure 10. Proton conductivity of membranes under different relative humidities (RHs) at 80°C. The hybrid membranes were named after Nafion/phytic@ MIL-X or Nafion/pure-MIL-X, where phytic@MIL or pure-MIL referred to the filler in hybrid membranes, respectively, and X referred to the weight percentage of phytic@MIL101 or pure-MIL101 relative to Nafion. Reprinted with permission from reference 76. Copyright 2014 American Chemical Society.

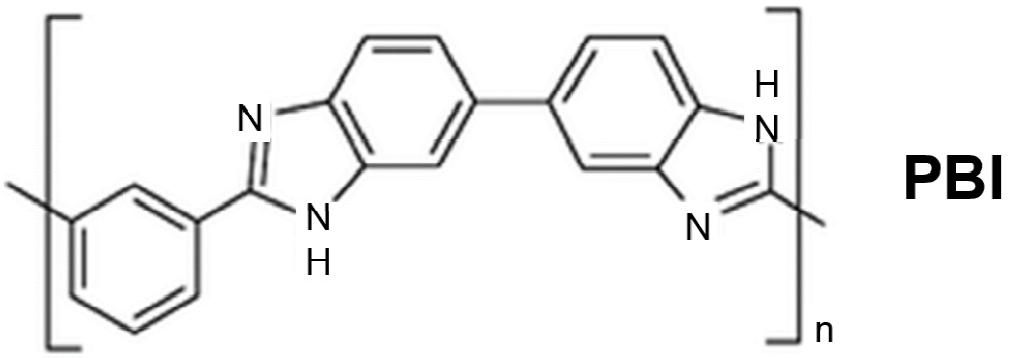

Figure 11. Chemical formula for a typical PBI compound. Adapted from reference 81 with permission from The Royal Society of Chemistry.

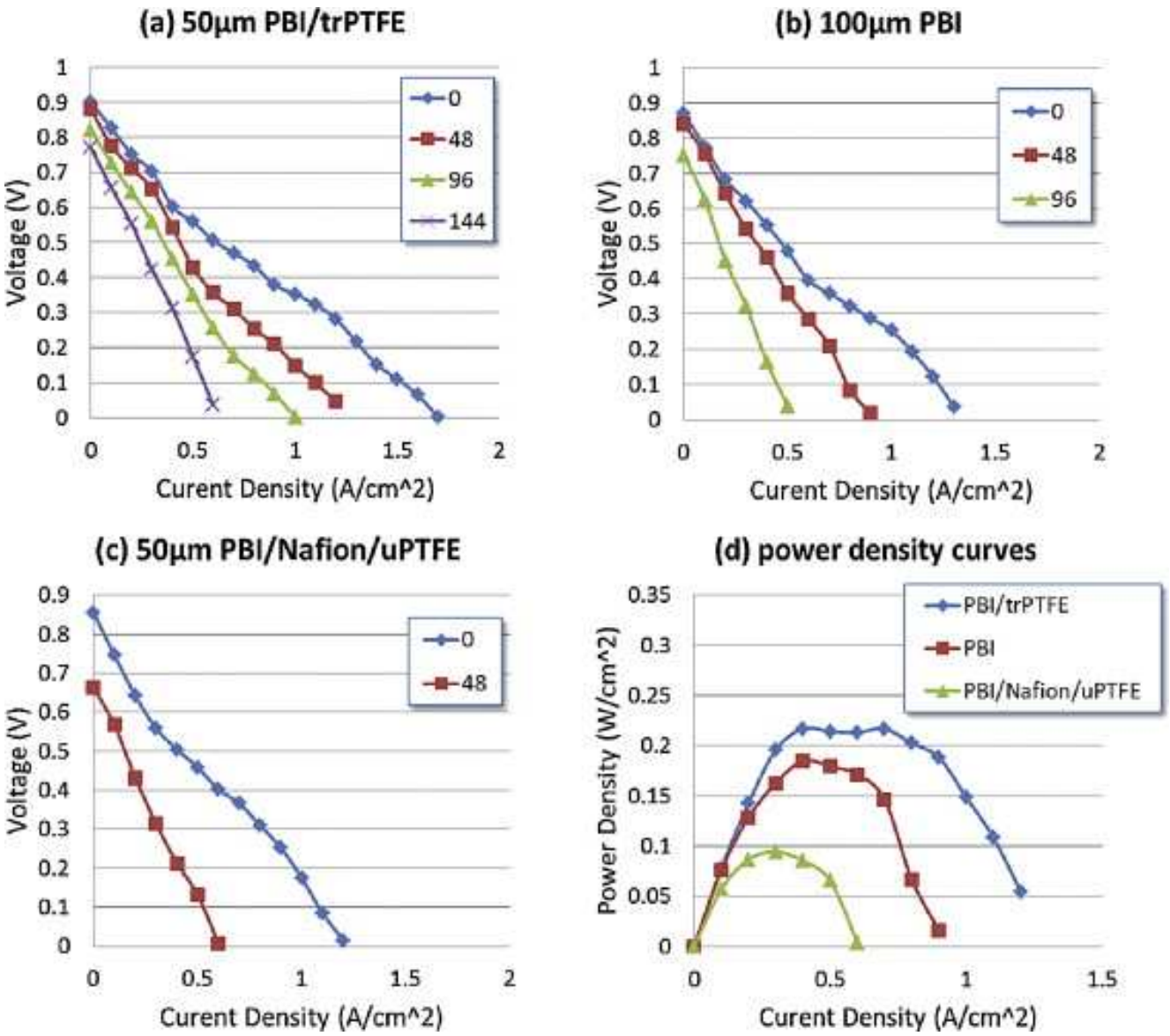

Figure 12. Fuel cell performance of MEAs with (a) PBI/trPTFE, (b) 100 µm PBI-only, and (c) PBI/Nafion/uPTFE membrane during the accelerated degradation process. (d) Power density curves obtained at 48 cycles. Reprinted with permission from reference 84. Copyright 2014 Elsevier B.V.

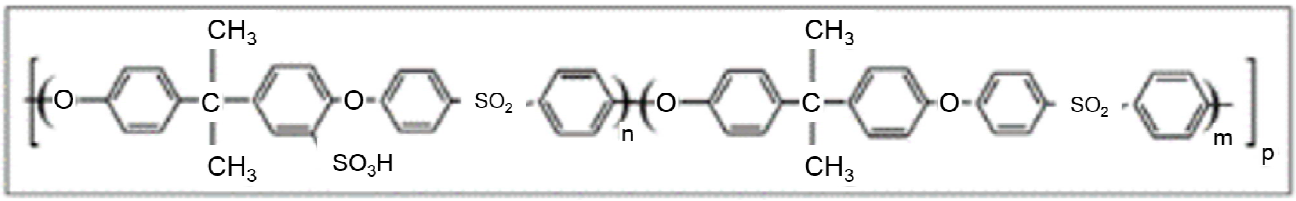

Figure 13. Representative chemical formula of a sulfonated polysulfone. Reprinted with permission from reference 73. Copyright 2014 American Chemical Society.

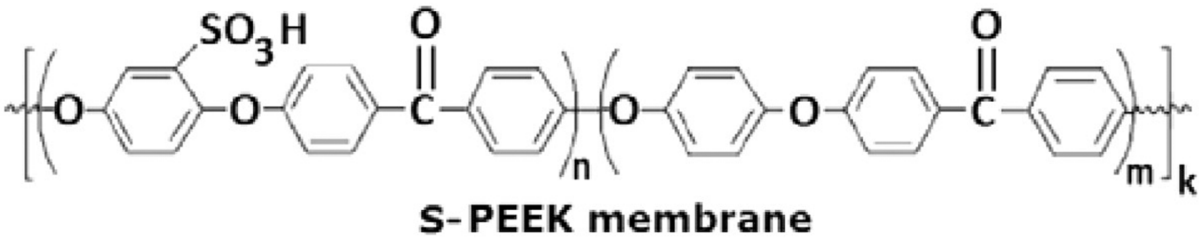

Figure 14. Representative formula of sulfonated poly(ether ketone). Reprinted with permission from reference 73. Copyright 2014 American Chemical Society.

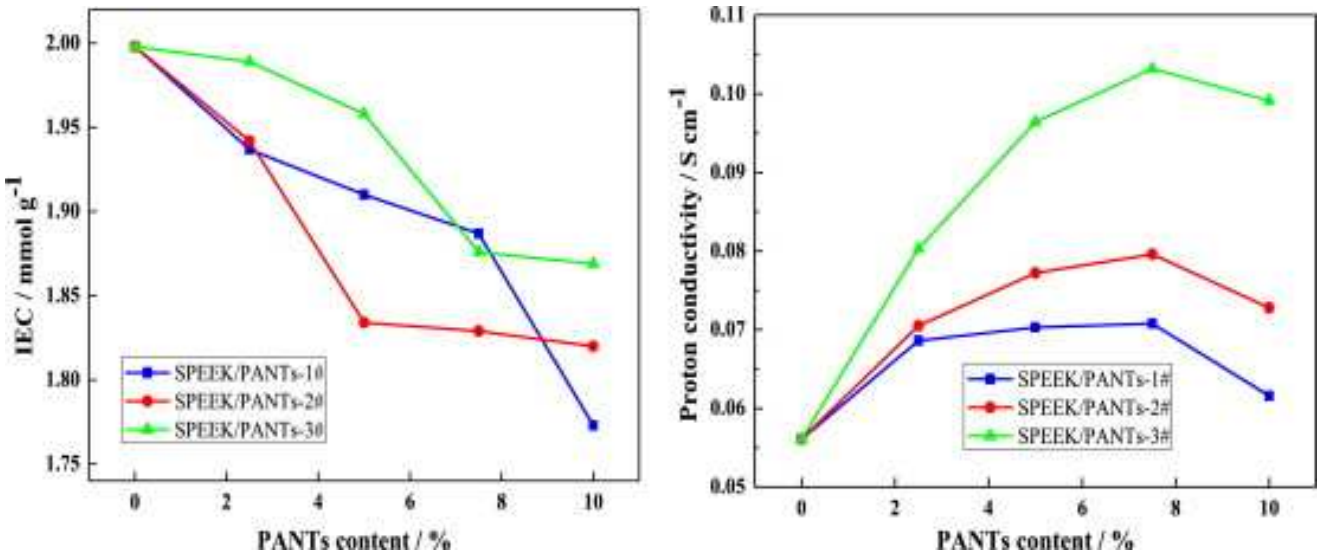

Figure 15. Ion exchange capacity (IEC) and proton conductivity of the membranes at 30°C. The composite membranes were designated as SPEEK/PANTs-N-X, where N (= 1, 2, or 3, for example) represented the type of the synthesized PANTs and X (= 2.5, 5, 7.5, or 10) was the weight percentage of the fillers to SPEEK. Reprinted with permission from reference 89. Copyright 2014 Elsevier B.V.

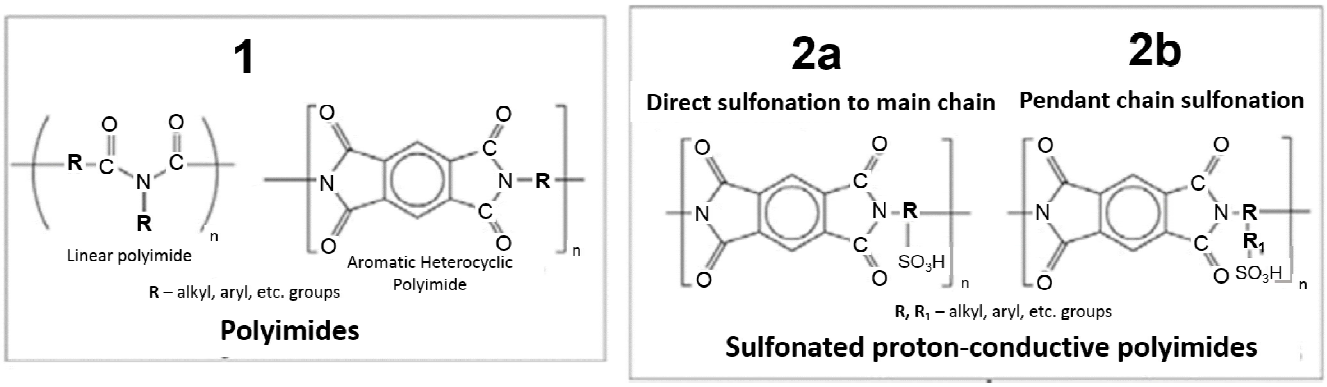

Figure 16. (1) Polyimides, sulfonated polyimides with (2a) sulfonated main chains and (2b) sulfonated pendant chains. Reprinted with permission from reference 73. Copyright 2014 American Chemical Society.

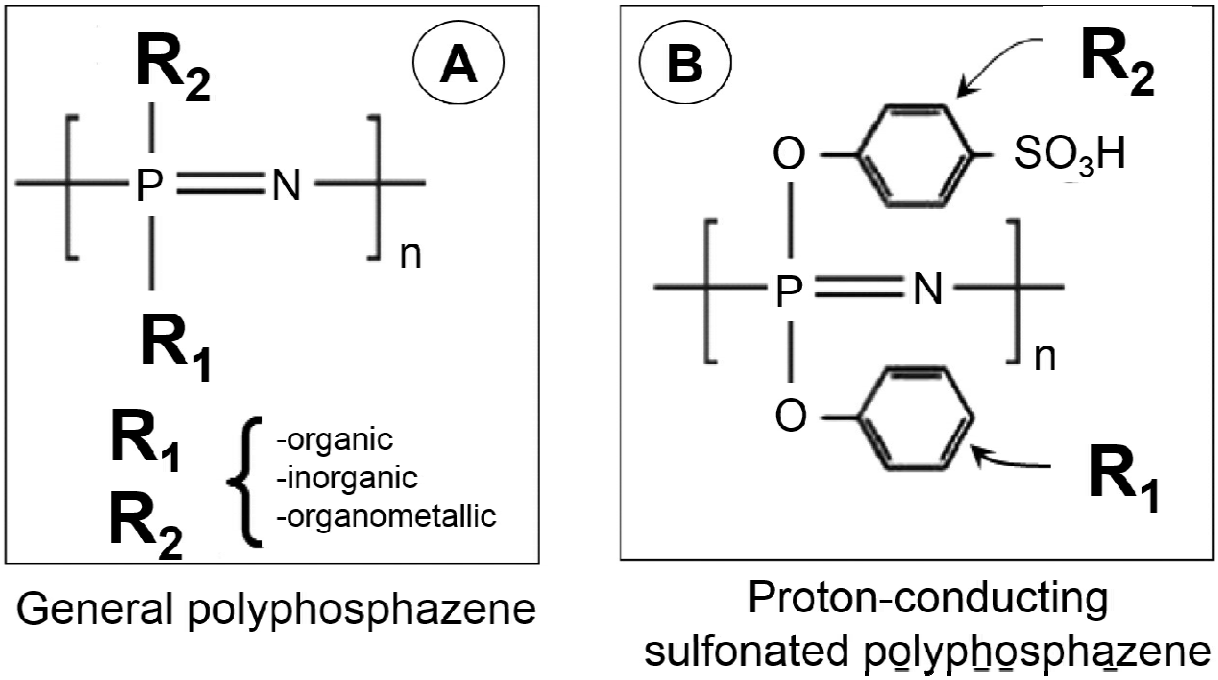

Figure 17. Generalized molecular structure of (A) polyphosphazene and (B) sulfonated polyphosphazene. Adapted with permission from reference 73. Copyright 2014 American Chemical Society.

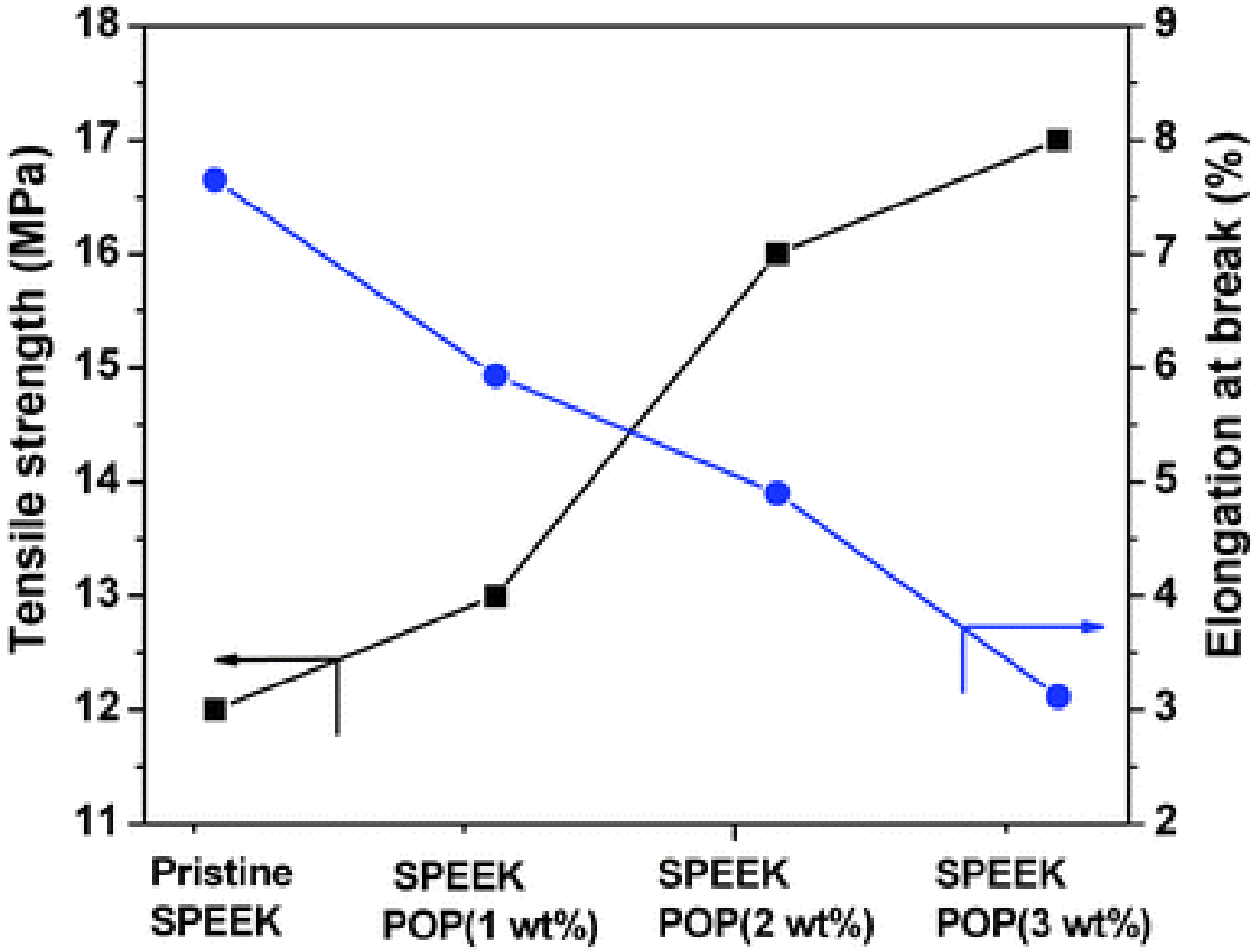

Figure 18. Graph depicting tensile strength as well as elongation at breakage as a function of polyphosphazene weight %. Reproduced from reference 81 with permission from The Royal Society of Chemistry.

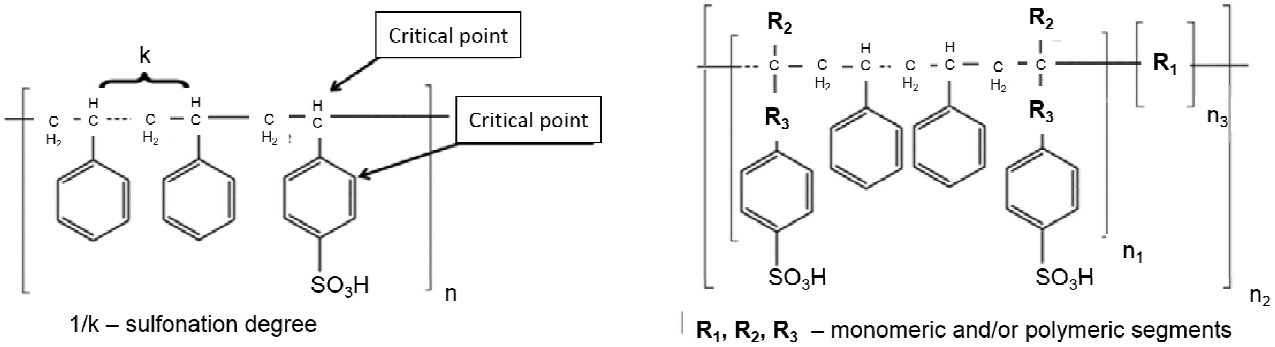

Figure 19. Chemical structure of functionalized PSSA membranes. Reprinted with permission from reference 73. Copyright 2014 American Chemical Society.

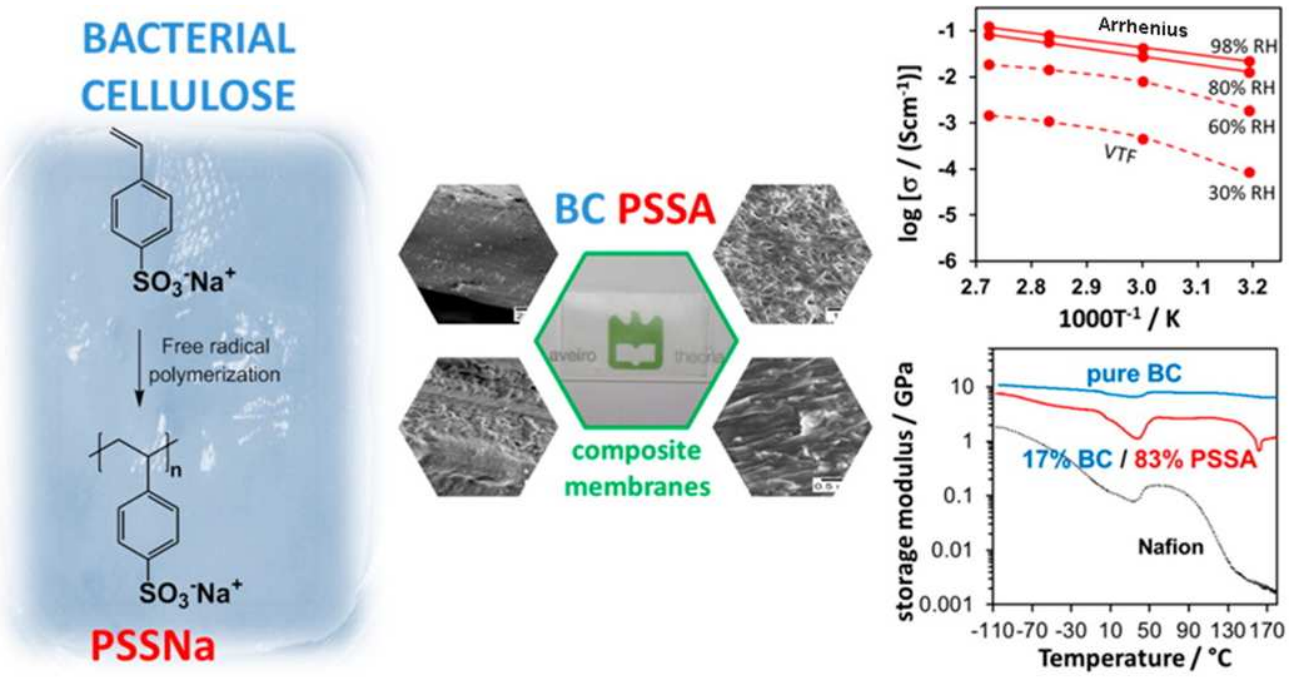

Figure 20. Left and middle portions designate the structures of the composite membrane. Right portion shows Arhhenius plot and storage modulus of the composite as well as of the control membranes. Reprinted with permission from reference 92. Copyright 2014 American Chemical Society.